USING EXTERNAL MAGNETIC FIELD FOR INCREASING STT-RAM READ/WRITE RELIABILITY

by

Enes Eken

Bachelor of Science, Selcuk University, Turkey, 2009

Submitted to the Graduate Faculty of

Swanson School of Engineering in partial fulfillment

of the requirements for the degree of

Master of Science in Electrical Engineering

University of Pittsburgh

2014

UNIVERSITY OF PITTSBURGH

SWANSON SCHOOL OF ENGINEERING

This thesis was presented

by

Enes Eken

It was defended on

March 27th, 2014

and approved by

Dr. Yiran Chen, Ph.D., Assistant Professor, Electrical and Computer Engineering Department

Dr. Steven P. Levitan, Ph.D., Professor, Electrical and Computer Engineering Department

Dr. Zhi-Hong Mao, Ph.D., Associate Professor, Electrical and Computer Engineering Department

Thesis Advisor: Yiran Chen, Ph.D., Assistant Professor,

Electrical and Computer Engineering Department

USING EXTERNAL MAGNETIC FIELD FOR INCREASING STT-RAM READ/WRITE RELIABILITY

Enes Eken, M.S.

University of Pittsburgh, 2014

In recent years, we have been witnessing the rise of spin-transfer torque random access memory (STT-RAM) technology. There are a couple of reasons which explain why STT-RAM has attracted a great deal of attention. Although conventional memory technologies like SRAM, DRAM and Flash memories are commonly used in the modern computer industry, they have major shortcomings, such as high leakage current, high power consumption and volatility. Although these drawbacks could have been overlooked in the past, they have become major concerns. Its characteristics, including low-power consumption, fast read-write access time and non-volatility make STT-RAM a promising candidate to solve the problems of other memory technologies. However, like all other memory technologies, STT-RAM has some problems such as cell-to-cell process variations and intrinsic thermal fluctuations which are waiting to be solved. In order to solve these variations and improve read/write reliability, we propose the utilization of an external magnetic field. When an external magnetic field is applied to a magnetic tunnel junction (MTJ) during a read operation, a self-reference resistive signal will be generated. This self-reference resistance is a very important technique for improving read reliability. In addition, external magnetic field can also be used for improving MTJ switching time.

TABLE OF CONTENTS

LIST OF TABLES

LIST OF FIGURES

ACKNOWLEDGEMENT

I would like to thank my advisor, Professor Yiran Chen, for his help and academic guidance throughout the research. Without his patience, I would never manage to write this thesis and most importantly, never learn how to research.

I really appreciate to Professor Steven Levitan and Professor Zhi-Hong Mao for spending their time as being my committee members.

I would also like to express my gratitude to our research group who helped me whenever I need assistance.

I would like to express the deepest appreciation to my family and my brothers for praying for me.

I am also very grateful to Government of the Republic of Turkey and Republic of Turkey Ministry of National Education whose generous grant made this study possible.

1.0 INTRODUCTION

Importance of on-chip embedded memory has been increasing day by day in parallel with multi-core architecture. In order to meet this growing demand, conventional memory technologies, e.g., SRAM, DRAM, Flash memory etc., have been commonly used. However, beyond 22nm technology node these charge based conventional technologies encounter significant problems like high leakage power consumption, process variation and intrinsic thermal fluctuations. In order to eliminate these problems, different memory technologies i.e. phase-change memory (PCM), magnetic memory (MRAM), resistive memory (ReRAM), spin-transfer torque random access memory (STT-RAM), etc., have been proposed. Among these technologies, STT-RAM has attracted a great deal of attention for its unique characteristics such as zero standby power consumption, fast read/write speed, high endurance and excellent CMOS-compatibility [1].

In an STT-RAM, binary data is stored in a magnetic tunneling junction (MTJ). An MTJ is a sandwiched structure which includes two ferromagnetic layers and between these two layers, one MgO tunneling barier as shown in Figure 1.1. One of these two ferromagnetic layers' magnetization direction is fixed. This layer is called as the reference or pinned layer. On the other hand, the second layer's magnetization direction can be switched by injecting a spin

polarized current or applying an external magnetic field. Therefore this layer is called as the free layer. In a magnetic tunneling junction (MTJ), a binary data is stored as a function of MTJ's

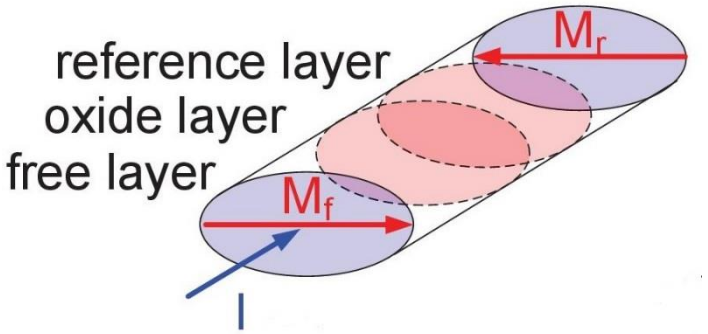

Figure 1-1: Illustration of an MTJ

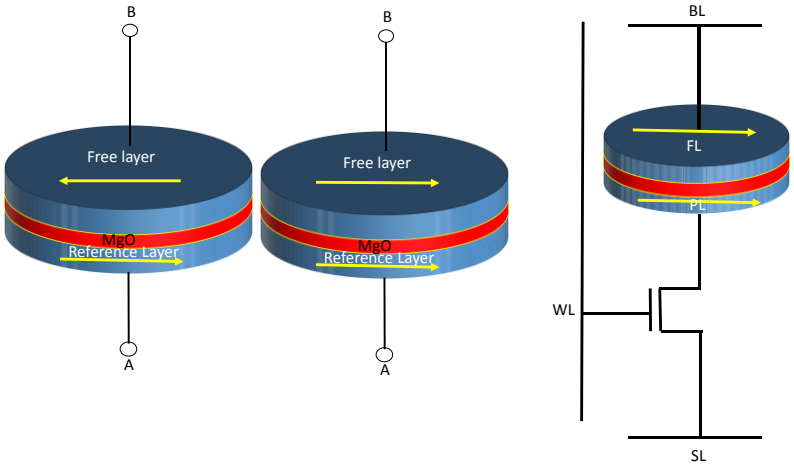

Figure 1-2: MTJ structure. (a) Anti-parallel (b) Parallel (c) 1 Transistor 1 MTJ cell structure.

resistance as shown in Figure 1.2. If the magnetization direction of the free layer is parallel to the pinned layer, resistance of the MTJ will be low which represents logic '0', on the contrary, if the free layer's magnetization is antiparallel, this time the MTJ's resistance will be high which represents logic '1'. Figure 1.2 (c) shows the most commonly used 1 transistor 1 MTJ (1T1J) cell structure as MTJ's free layer is connected to the bit line (BL) and reference layer is connected to the NMOS transistor, transistor's gate is connected to the word line (WL) in order to choose related bit. Third terminal of the transistor is connected to source line (SL).

If a positive voltage is applied to the BL, current will flow the BL to the SL, however electron charges will flow from the SL to the BL as shown in Figure 1.3(a). While electrons are going through pinned layer, electrons which have same spin direction with the pinned layer can pass the pinned layer and become a spin polarized current. The polarized current applies a torque to the free layer's magnetization direction and switches it from the antiparallel state to the parallel state. Electrons which have opposite spin direction with the pinned layer cannot pass and they are reflected. In the reverse of this condition, if a positive voltage is applied to the SL, the

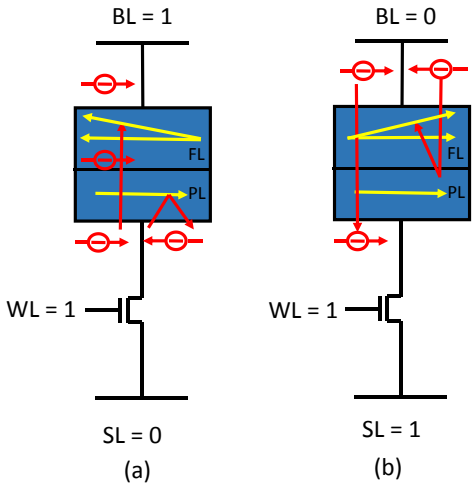

Figure 1-3: MTJ Switching (a) From anti parallel to parallel. (b)From parallel to anti parallel

current will flow from free layer to the pinned layer. This time, since the free layer's magnetization direction is not so strong all of the electrons can pass the free layer and come to the pinned layer. In the same manner, electrons which have the same spin direction with the pinned layer's magnetization direction can keep going on their way, however electrons which have the opposite spin direction with the pinned layer will be reflected. These reflected electrons apply a torque to the free layer and switches the free layer's direction from the parallel to the anti parallel state.

Although STT-RAM is a very promising candidate for future memory technologies with its high density, high scalability, low power consumption and fast read/write operation features, like all other nano-scale technologies, STT-RAM also faces great challenges with cell-to-cell variations and intrinsic thermal fluctuations. In the read operation, resistance sense margin plays a very important role because, a small sense margin causes false detections. However wide variation of the MTJ resistance limits this sense margin [2]. In addition, ambient temperature decreases critical switching current such that read current (which is less than switching current in normal operation) can inadvertently switch the MTJ. Furthermore, ambient temperature also affects write speed.

In this work we propose to use an external magnetic field. If an external magnetic field is applied to an MTJ device, a self-reference resistive sense signal can be generated. We named this novel method "field-assisted access scheme of STT-RAM (FA-STT)". Simulation results show that our scheme is more robust for process variation and therefore improves read reliability and increases write speed.

1.1 THESIS OUTLINE

The rest of this thesis is organized as follows: The basics of STT-RAM is presented in Section I. Section II explains the background of the STT-RAM and magnetization dynamics based on the Landau-Lifshitz-Gilbert equation, Section III shows different STT-RAM cell structures and read/write operations. Section IV depicts details of the field-assisted access scheme of STT-RAM (FA-STT). Methodology is presented in Section V and conclusions are given in Section VI.

2.0 BACKGROUND AND MAGNETIZATION DYNAMICS

This section gives some general information about the magnetization dynamics of the free layer which is model by the Landau-Lifshitz-Gilbert (LLG) equation. Earlier version of the LLG equation is shown in equation 2.1 and this equation is developed for toggle magnetic ram which only considers switching the free layer's magnetic moment direction by applying an external

$$\frac{d\mathbf{M}}{dt} = -\gamma_0(\mathbf{M}\times\mathbf{H}) + \frac{\alpha}{\mathrm{M}_S}\mathbf{M}\times\frac{d\mathbf{M}}{dt} \tag{2.1}$$

magnetic field but not by injecting current. In the equation 2.1, **M** is free layer's magnetic moment vector, M_s is the magnetization saturation, **H** is the effective magnetic field vector, α is the Gilbert damping constant, γ_0 is the gyromagnetic constant.

H, effective magnetic field, is the summation of different magnetic fields which are affecting the free layer's magnetic moment [7]. **H** can be represented as;

$$\mathbf{H} = \mathbf{H}_a + \mathbf{H}_k + \mathbf{H}_p$$

in which $\mathbf{H}_a$ is the external magnetic field, $\mathbf{H}_p$ is the easy plane effective field, $\mathbf{H}_k$ is the uniaxial anisotropy field, in the absence of any external force free layer's magnetic moment prefers to align itself in one axis which is called as easy axis (positive or negative direction which is the same with the pinned layer's magnetic moment direction). If the free layer's

magnetic moment is not collinear with easy axis, uniaxial anisotropy field wants to pull free layer's magnetic moment back to easy axis.

Later, effect of spin polarized current's capability for switching the free layer's magnetic moment was discovered and a spin torque term was added to the original form of the equation. Modified LLG equation [3]-[6] is shown in equation 3.2:

$$\frac{d\mathbf{M}}{dt} = \underbrace{-\gamma_0(\mathbf{M}\times\mathbf{H})}_{\Gamma_{\text{precession}}} + \underbrace{\frac{\alpha}{M_S}\mathbf{M}\times\frac{d\mathbf{M}}{dt}}_{\Gamma_{\text{damping}}} + \underbrace{\frac{\gamma\eta J\hbar}{e\mu_0 M_s d}\mathbf{M}\times(\mathbf{M}\times\mathbf{m}_p)}_{\Gamma_{\text{spin}}} \quad (3.2)$$

Third term of right hand side (RHS) of the LLG equation is representing the effect of the spin torque in which, γ is the gyromagnetic ratio, $\hbar$ is the Planck constant, n spin polarization factor, J is the current density, μ is the permeability, d is the thickness of the free layer, e electron value and $\mathbf{m}_p$ is the pinned layer's magnetization direction.

2.1 COMPONENTS OF THE LLG EQUATION

It is possible to divide this equation into three parts to make it simple to explain as "damping torque", "spin torque" and "precession torque" as shown in Figure 2.1. Each of these torques will be explained one by one by giving the simulation results. Theoretical details of these torques will be given in Section 5.

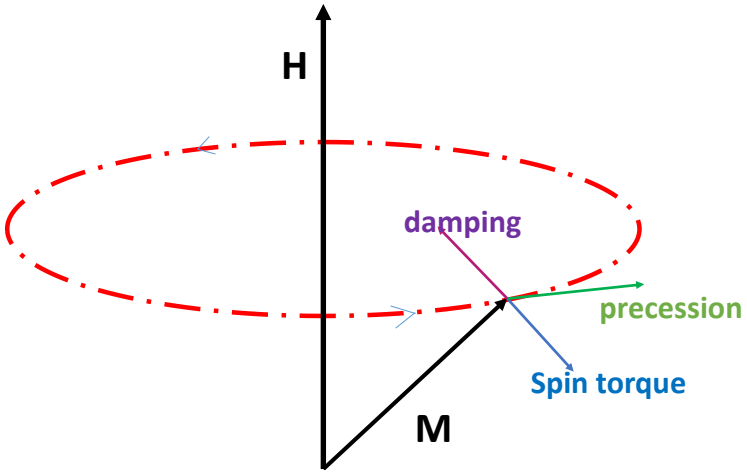

Figure 2-1: Components of LLG equation

2.1.1 Precession Torque

If a free layer's magnetic moment is exposed to a magnetic field, the free layer's magnetic moment starts to precess. Precession can be introduced as the cross product of the magnetic moment vector (**M**) and the effective magnetic field vector (**H**). The result of this cross product will give the precession torque which is perpendicular to both **M** and **H** vectors and this torque pulls the magnetic moment vector around the effective magnetic field. By ignoring damping torque and spin torque, we can observe the effect of the precession as shown in Figure 2.2. Since magnitude of the free layer's magnetic moment vector is constant, one can say that precession must be symmetric and it must be like a circle as shown in Figure 2.2. However easy plane

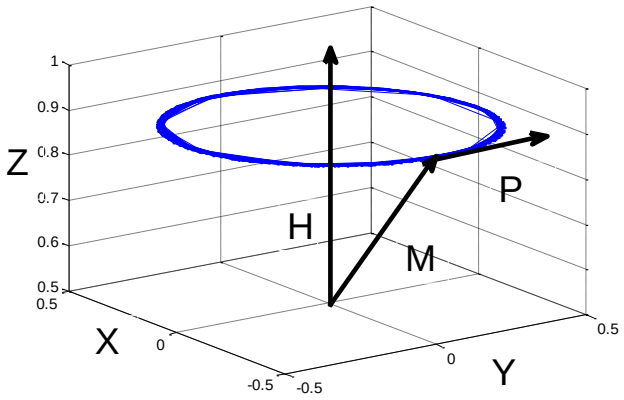

Figure 2-2: Precession torque

anisotropy prevents magnetic moment's motion in a plane and does not allow it go out from this y-z plane. While simulating the Figure 2.2, we cancelled easy plane anisotropy, but in reality, easy plane anisotropy must be considered. By taking into account this anisotropy, new simulation will be like in Figure 2.3.

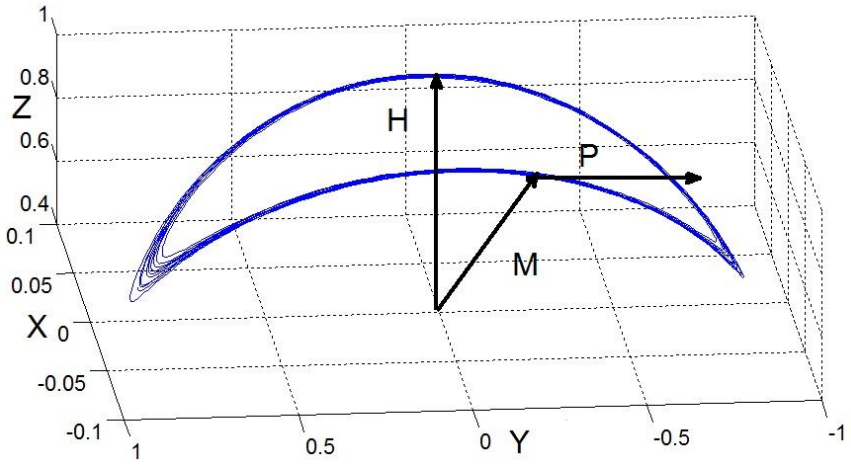

Figure 2-3: Effect of easy plane to precession

2.1.2 Damping Torque

Second term on the right hand side of the LLG equation is the damping torque. During the

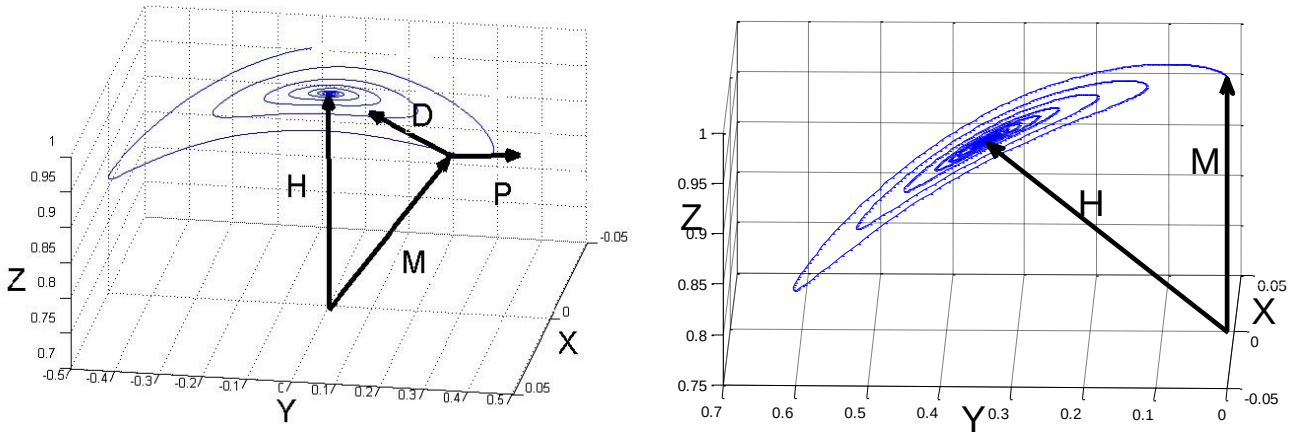

Figure 2-4: Damping torque. (a)H is applied in Z axis. (b) H makes an angle with Z axis

precession, the free layer's magnetic moment will dissipate energy until the amplitude of the precession will be zero which means the magnetic moment will align to the applied field [4]. When the magnetic moment is subjected to a magnetic field, the effect of the damping torque can be seen by taking into account the precession and damping torque and ignoring spin transfer torque. As shown in Figure 2.4, after the precession, the magnetic moment dissipates its energy and finally the free layer gets damping and lies in the direction of applied magnetic field vector **H**. In Figure 2.4(a), the magnetic field is applied in the direction of the z axis so, the free layer's magnetic moment gets merged with the **H** vector. If the **H** vector's direction changes, the magnetic moment will align itself into new position.

As can be seen from Figure 2.4(b), **M** deviates from its original position and merges with the **H** vector. As mentioned in the first part, the resistance of the MTJ is a function of θ, the angle between the free layer's magnetic moment and the pinned layer's magnetic moment. Since the θ is changed, the resistance is also changed.

After displacing the free layer's magnetic moment as shown in Figure 2.5, when the external magnetic field is removed, the free layer's magnetic moment bounces back and comes to its original position. For this simulation first **H** is applied and **M** lies collinear by following the red precession. Then **H** is removed and **M** comes back to its original position by following the blue precession.

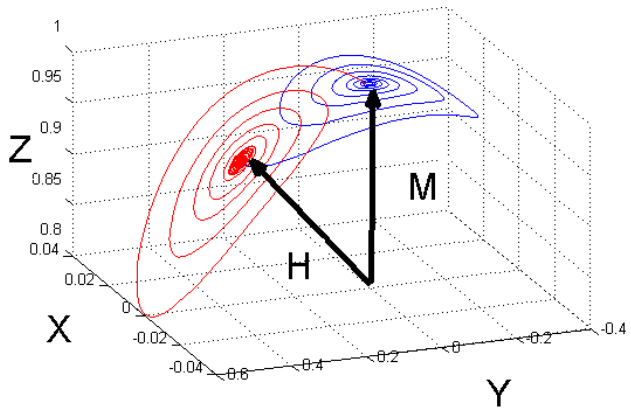

Figure 2-5: Motion of the free layer's magnetization under a magnetic field

2.1.3 Spin Torque

The third and final term of the RHS of the LLG equation is spin torque. When a current is injected into the ferromagnetic layer, this current generates a torque and this generated torque is

absorbed by the free layer's magnetic moment. Depending on the sign of the applied current, the torque either increases or decreases the magnitude of the precession [6]. If the injected current is big enough, the free layer will switch.

After combining all of these three torque terms, the dynamic response of the free layer's magnetic moment can be modeled. Switching of the free layer from state 0 to state 1 due to injected current can be seen from Figure 2.6. In the original position (in state 0) magnetic moment makes much more precession comparing with state '1' because, in state '0', damping torque and spin torque fight each other which causes more precession. On the other hand after

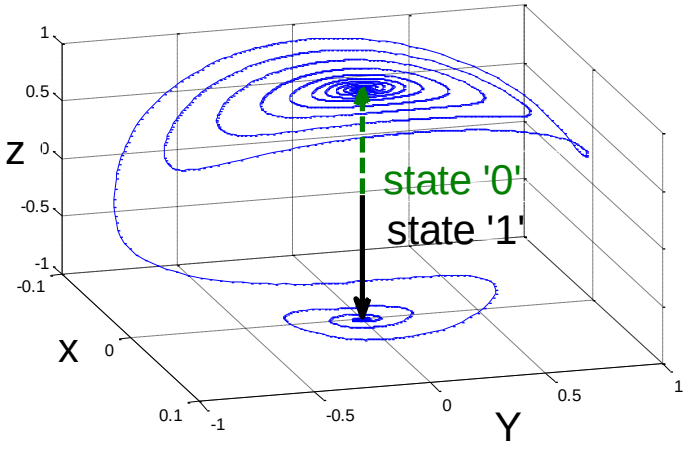

Figure 2-6: MTJ switching in 3D

magnetic moment reaches right angle (90^{o}), damping torque switches its direction and this time damping torque helps the spin torque which causes less precession. Because of the simplicity, instead of using a 3D figure, a 2D figure is more commonly used for showing switching. In 2D figures only the z axis is considered since magnetic moment's easy axis is the z axis. 2D motion can be seen in Figure 2.7.

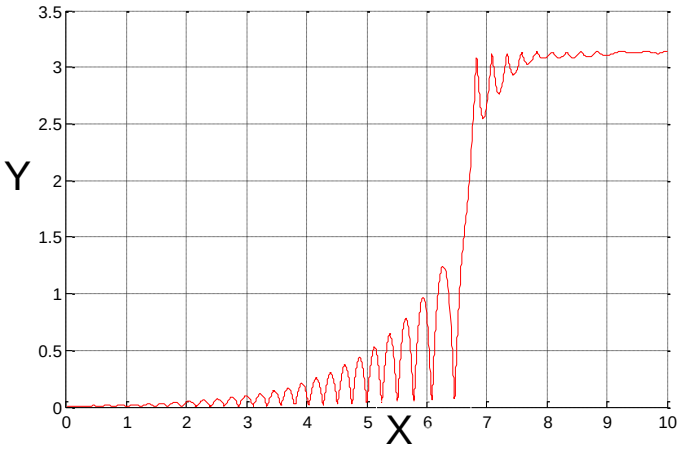

Figure 2-7: MTJ switching in 2D

2.2 FACTORS AFFECTING SWITCHING AND PRECESSION TIME

There are some factors which affect the precession and switching time. Gilbert damping constant α is one of these factors. A bigger alpha results in a faster switching. The effect of α can

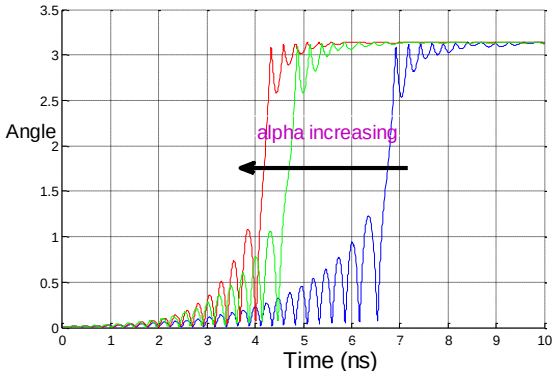

Figure 2-8: Effect of α to switching time

be seen from Figure 2.8. The Gilbert damping constant is not the only way to increase switching speed. If the effective magnetic field is increased, precession will be much faster. One way to create a bigger effective field is to apply an external magnetic field. Simulation results for different magnitudes vs. switching time can be seen from Figure 2.9.

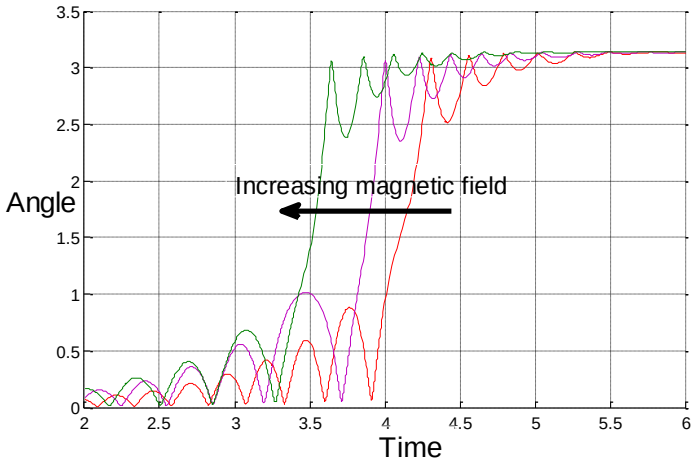

Figure 2-9: Effect of the magnetic field on switching time

3.0 STT-RAM CELL STRUCTURES AND OPERATIONS

One of the technical challenges of STT-MRAM is the read operation due to MTJ process variation and thermal fluctuation. Any variation on MTJ resistance directly affects the read operation. Moreover MTJ resistance is very vulnerable to the device parameters such as thickness of the oxide barrier in the MTJ. For instance changing of this thickness from 14A to 14.1A increases the MTJ resistance 8% [8]. Until now different read operation techniques have been suggested. Three of them are the conventional voltage sensing scheme, the conventional self-reference scheme and the nondestructive self-reference scheme.

3.1 CONVENTIONAL VOLTAGE SENSING SCHEME

The most elementary and earliest technique among the already existing techniques is the conventional voltage sensing scheme as shown in Figure 3.1.

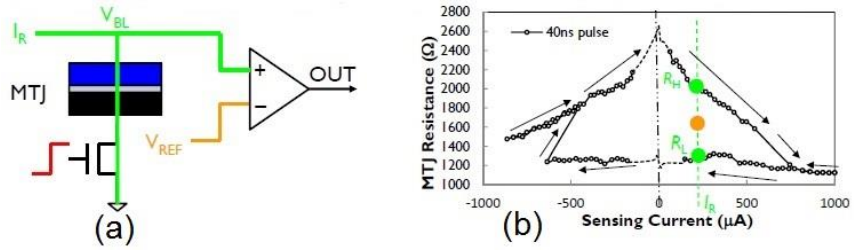

Figure 3-1: (a) Conventional voltage sensing scheme. (b) I-R curve of MTJ [9]

This technique is based on two steps. First a read current I_R is applied to the bit line (BL) to generate a voltage. Depending on the resistance state of the MTJ being low or high, BL voltage will be

$$V_{BL,L} = I_R*R_L \text{ or } V_{BL,H}=I_R*R_H, \quad (3.1)$$

respectively. This generated voltage is stored in a capacitor which top is connected to the sense amplifier. As the next step, this generated voltage is compared with a pre-defined reference voltage. If the BL voltage is bigger than the reference voltage, data is logic '1', reverse of this condition means logic '0'. Even though this technique is very straightforward, it has a demerit at defining the reference voltage point. Because of the MTJ process variation, there is not such a guarantee that every MTJ's low resistance is lower than the reference value or every MTJ's higher resistance is higher than the reference value. An MTJ's both high and low resistances can be lower or higher than the reference value actually which means that MTJ will be read constantly state '1' or '0'. Due to this problem, people aboundened this technique and proposed to use self-reference technique.

3.2 SELF-REFERENCE READ SCHEME

Self-reference read scheme is another technique [10] which utilizes the fact that an MTJ's low state resistance is always lower than its own high state resistance. The schematic can be seen

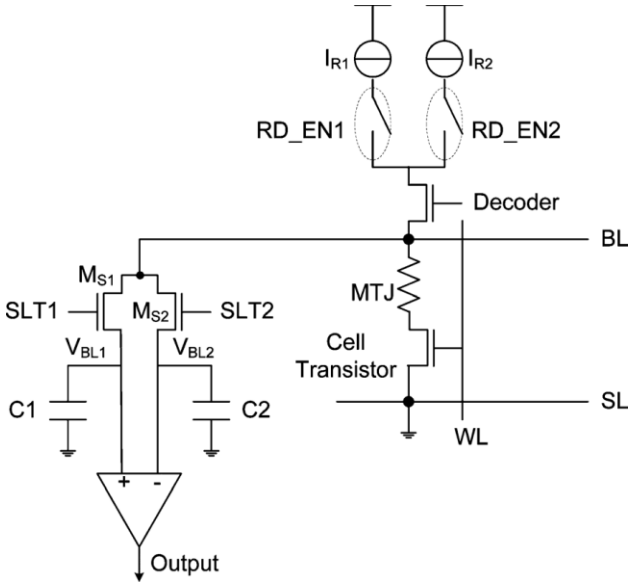

Figure 3-2: Self-reference read scheme [10]

in Figure 3.2. This technique has four steps. First the original data stored in the MTJ should be sensed by applying I_{R1} current and stored in a capacitor C1. Then a reference value such as state 0 should be written to the MTJ. As a third step another read current I_{R2} which is bigger than I_{R1} should be applied and the generated voltage should be stored in capacitor C2. After this step, the original data and latterly written reference data should be compared as a function of voltage. If the original voltage is higher than the reference voltage, it means it is logic 1, reverse of this condition means logic 0. For the last step, since a data is written over the original one, the original one should be written back. Even though this technique provides much more certain result comparing with the voltage sensing scheme, there are still some problems. In this technique MTJ should be read two times and should be written two times. Obviously these two read and write operations will take a huge amount of time comparing with the other scheme. In addition this technique is much more energy hungry especially taking into account that writing

operation consumes very high energy. On the other hand if the energy is shut down before the last step (the step of writing back the original data), original data will be lost. This is a very big concern for non-volatile memory and because of writing a reference value over the original one, this technique is also called as destructive self-reference scheme.

3.3 NON-DESTRUCTIVE SELF-REFERENCE READ SCHEME

The most recently proposed technique is non-destructive self-reference read scheme. Instead of utilizing the differences between high and low resistance which is mentioned above, this scheme benefits the I-R curve of an MTJ.

As can be seen from the Figure 3.1(b), an MTJ's high resistance curve is much more stepper than the low resistance curve. A small change in a read current gives much more deviation for the high resistance than the low resistance. So realizing this principal, a read current I_1 is applied to generate a BL voltage as

$$V_1 = I_1 * R_1. \tag{4.2}$$

This voltage stored in a capacitor. Next another read current I_2 which is almost double of I_1 is applied and generates a second voltage as

$$V_2 = I_2 * R_2 = 2 * I_1 * R_2 . \tag{4.3}$$

Then by using a ½ voltage divider we can reach

$$V_{2O} = I_1 * R_2. \tag{4.4}$$

The differences between V_1 and V_{2O} will be

$$\Delta V_{BL} = V_1 - V_{2O} = I_1 * (R_1 - R_2). \tag{4.5}$$

At this point, we refer again I-R curve of the MTJ. As can be seen from the Figure 3.1(b), for state 1, while difference between R1- R2 is bigger than zero, for state 0, the difference will be almost 0. The biggest this advantage of this method is that I_2 is almost double of I_1. This increases the probability of disturbing the stored data.

4.0 FIELD-ASSISTED ACCESS SCHEME OF STT-RAM (FA-STT) [1]

As we briefly mentioned in the introduction part, we propose external magnetic field-assisted STT-RAM (FA-STT) design to improve the read and write reliability. Figure 4.1(a) illustrates the FA-STT design.

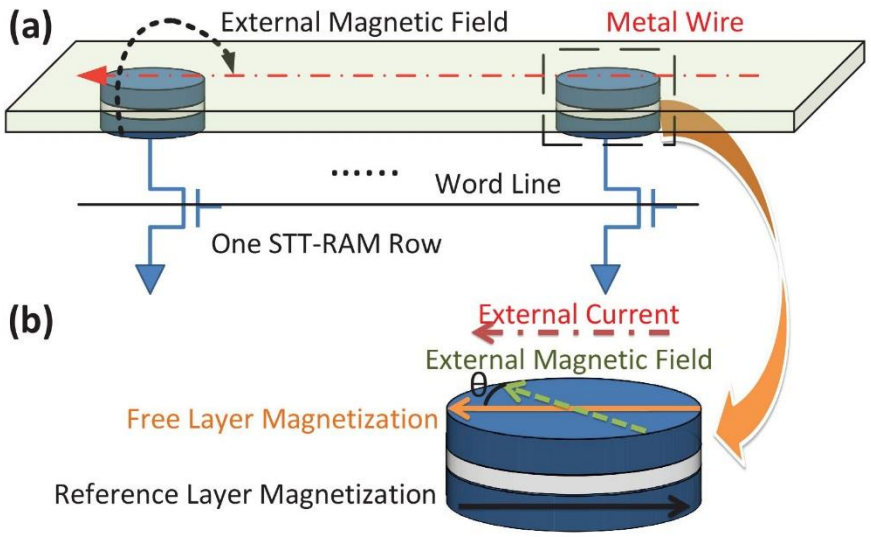

Figure 4-1: (a) 3D view of FA-STT scheme. (b) MTJ intermediate resistance state generation.

[1] The content of this chapter is based on the publication of [16] and has been customized for this thesis.

As can be seen from Figure 4.1(a) a row of memory cells share the same word-line control and an extra metal wire is placed above the entire row.

There is not an electrical connection between metal wire and MTJs. By injecting a current to the metal wire, an external magnetic field will be generated. This magnetic field exerts a torque to the MTJ's free layer magnetization and as a result, free layer's magnetization deviates from its original parallel or anti parallel position to a reference position as shown in Figure 4.1(b).

4.1 THEORY OF FA-STT

MTJ resistance is a function of relative angle θ between pinned layer's and free layer's magnetizations. The angular dependence of the magneto-resistance in an in-plane MTJ can be described as [13]:

$$R(\theta) = R(0) + \Delta R \frac{1-\cos\theta}{2+\lambda(1+\cos\theta)}, \tag{4.1}$$

where, λ is fitting parameter.

While in state 1, since the pinned layer and the free layer are in opposite direction, θ will be 180^o and resistance will be maximum. In state 0, this time θ will be 0^o and resistance will be minimum. In state 1, if the angle is reduced a fixed value, this will decrease the resistance of the MTJ to an intermediate value.

On the other hand, in state 0, if the angle increases, it will increase the resistance of the MTJ to an intermediate value. An external magnetic field is capable to change this angle so the resistance. How much θ will change is an issue of the magnitude of the applied field. In a read

operation, a judgment can be done by comparing the original resistance and the intermediate resistance. If the original resistance is greater than the intermediate resistance, it means stored data is logic 1, reverse of this means logic 0.

In an MTJ, a free layer is mainly under the effect of four energy landscapes: uniaxial anisotropy, easy plane anisotropy, Langevin random field and applied magnetic field. Under these four energy landscapes, the free layer's magnetic orientation makes a precession. The motion of the free layer under these energy landscapes can be defined by the coordinates (θ, φ) angles respectively z axis and the x axis at any instant of time as shown in Figure 4.2. Since the magnetization is assumed to be constant in magnitude, the free layer magnetization can be introduced as

$$\boldsymbol{m_f} = \sin\theta\ \cos\varphi\ \overrightarrow{e_x} + \ \sin\theta\ \sin\varphi\overrightarrow{e_y} + \ \cos\theta\ \overrightarrow{e_z} \tag{5.2}$$

In the same manner external magnetic field vector which is created by the metal layer placed

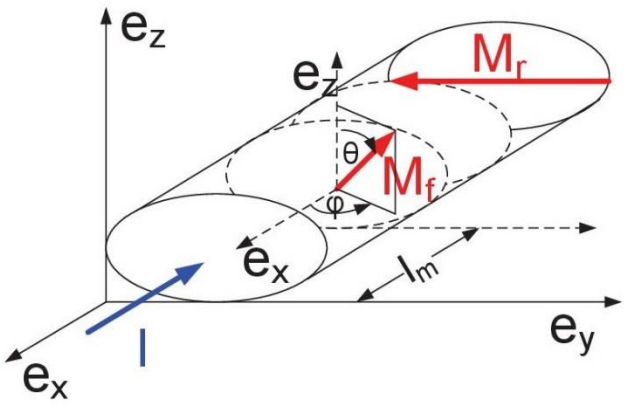

Figure 4-2: MTJ magnetization vector

over the MTJ, can be defined by (θ_H, φ_H) angles in the same coordinate system. Energy landscape experienced by the free layer's magnetization due to the applied magnetic field can be described as [14];

$$U_H = -\boldsymbol{M} \bullet \boldsymbol{H} = -MH(\sin\theta\cos\varphi(-\cos\theta_H) + \sin\theta\sin\varphi(\sin\theta_H\cos\varphi_H) + \cos\theta(\sin\theta_H\sin\varphi_H) \quad 5.3$$

Since the exerted torque by the external magnetic field is cross product of magnetic field vector and the magnetization vector, for the biggest value, magnetic field vector should be orthogonal to the magnetization orientation of the MTJ reference layer.

The torque which will be experience by the free layer magnetization can be determined by this formula [14]:

$$\frac{\boldsymbol{\Gamma}_U}{l_m K} = -m_f \times \nabla U_{\mathrm{H}}(\theta, \varphi) \tag{4.4}$$

with

$$\nabla U_{\mathrm{H}}(\theta, \varphi) = (\frac{\partial \mathrm{U}}{\partial \theta})\mathbf{e}_\theta + (\frac{1}{\sin\theta})(\frac{\partial \mathrm{U}}{\partial \varphi})\mathbf{e}_\varphi \tag{4.5}$$

where $\mathbf{e}_\theta$ and $\mathbf{e}_\varphi$ are unit vectors for θ and φ rotation respectively [14]. The torque will be

$$\frac{\Gamma_U}{l_m K} = -2h[(\sin\theta\sin\varphi\sin\theta_H\sin\varphi_H - \cos\theta\sin\theta\cos\varphi_H)\mathrm{e}_x - (\cos\theta\cos\theta_H + \sin\theta\cos\varphi\sin\theta_H\sin\varphi_H)\mathrm{e}_y + (\sin\theta\cos\varphi\sin\theta_H\cos\varphi_H + \sin\theta\sin\varphi\cos\theta_H)\mathrm{e}_z] \tag{4.6}$$

Here h is normalized value of magnetic field by uniaxial anisotropy field. Substituting this torque term into the LLG equation, we obtain two ordinary differential equations for coordinates

(θ, φ) to describe the motion of the magnetization vector of free layer due to the applied field as:

$$\begin{bmatrix} \theta' \\ \varphi' \end{bmatrix} = \begin{bmatrix} \left\{ \begin{matrix} -\alpha[\cos\theta\cos\varphi(-\cos\theta_M) + \cos\theta\sin\varphi\sin\theta_M\cos\varphi_M - \sin\theta\sin\theta_M\sin\varphi_M] \\ +[-\sin\varphi\cos\theta_M + \cos\varphi\sin\theta_M\cos\varphi_M] \end{matrix} \right\} \\ \left\{ \begin{matrix} [-\cos\theta\cos\varphi(-\cos\theta_M) - \cos\theta\sin\varphi\sin\theta_M\cos\varphi_M + \\ \sin\theta\sin\theta_M\sin\varphi_M] - \alpha[-\sin\varphi\cos\theta_M + \cos\varphi\sin\theta_M\cos\varphi_M] \end{matrix} \right] / \sin\theta \right\} \end{bmatrix} \quad (4.7)$$

4.1.1 FA-STT Read Operation

Due to external magnetic field creates a new intermediate resistance between high and low resistance states of the MTJ, we can conduct a two-step sensing scheme to detect the data stored in the MTJ by comparing the relative change between the intermediate and the original resistance states of the MTJ. The conceptual schematic of the FA-STT read circuit is shown in Figure 4.3(a). Procedure of the self-reference sensing scheme can be summarized as follows:

1. First read: By applying a read current I_R to the MTJ, a bit line voltage V_1 will be generated. Depending on the stored data, V_1 will be either V_{1L} or V_{1H} when the MTJ is at the low or high resistance state respectively. This bit line voltage is stored in a capacitor C_1.
2. Intermediate state generation: As the second step, for generating an intermediate state, transistor R_{en2} is which is connected to the metal wire is turned on and by passing a

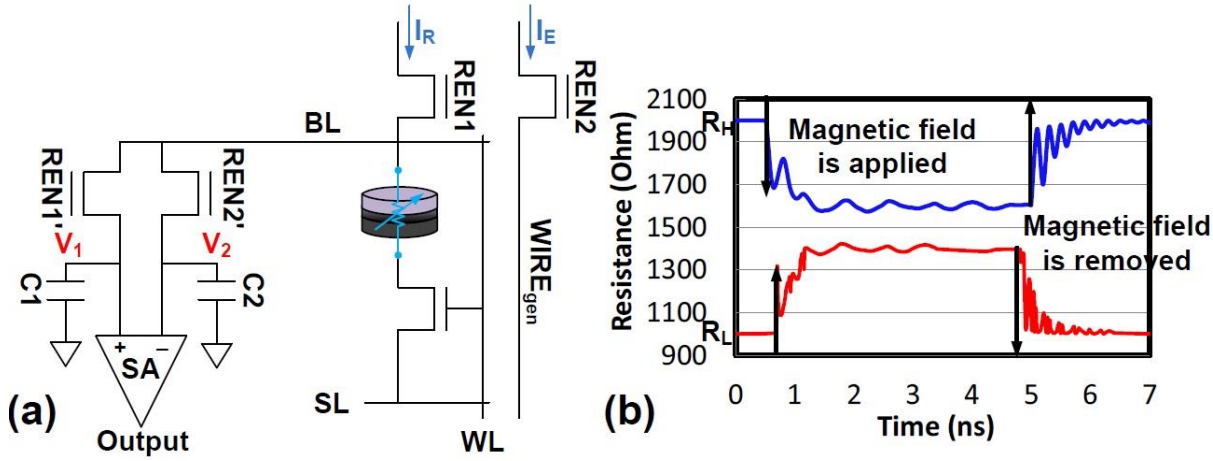

Figure 4-3: (a) Self-reference circuit design. (b) MTJ resistance during read operation.

current through $WIRE_{gen}$, an external magnetic field will be created. This magnetic field will force the free layer's magnetization to deviate from its original position, putting the MTJ into the intermediate state.

3. Second read: The same read current I_R is applied on the BL again and generates another BL voltage V_2. Depending on the MTJ's being low or high resistance, V_2 will be V_{2L} or V_{2H}. V_2 could be also stored in capacitor C_2. Since the intermediate state is between the low and high resistance state, we have $V_{2H} < V_{1H}$ and $V_{2L} > V_{1L}$.
4. Sensing: The data will be readout by comparing the voltages on two capacitors, i.e., '0' ($V_2 > V_1$) or '1' ($V_2 < V_1$).
5. Remove magnetic field: After sensing step is completed, the external magnetic field must be removed. As soon as the field is removed, free layer's magnetization orientation will bounce back to its original position after some oscillation. .

Figure 4.3(b) shows an example of the MTJ resistance change during our proposed self-reference sensing scheme. If stored data is logic '1', applied magnetic field decreases the

resistance value. If stored data is logic ‘0’, this time, applied field increases the resistance value. After removing the magnetic field, resistance of the MTJ bounces back to its original value.

4.1.2 Read Disturbance

In some conditions, even if MTJ read current is operated in secure point, thermal fluctuations can decrease the write current (critical current) value below the read current which means that read current can switch the MTJ. This condition is called as read disturbance. In the FA-STT sensing scheme, since the free layer’s magnetization is already displaced its original position and approached to 80^{o} in order to increase sensing margin, the probability of MTJ state flipping is aggravated.

As shown in Figure 4.4, applying external magnetic field, creates an oscillation on MTJ’s magnetization orientation and so MTJ resistance. However, due to damping factor of the

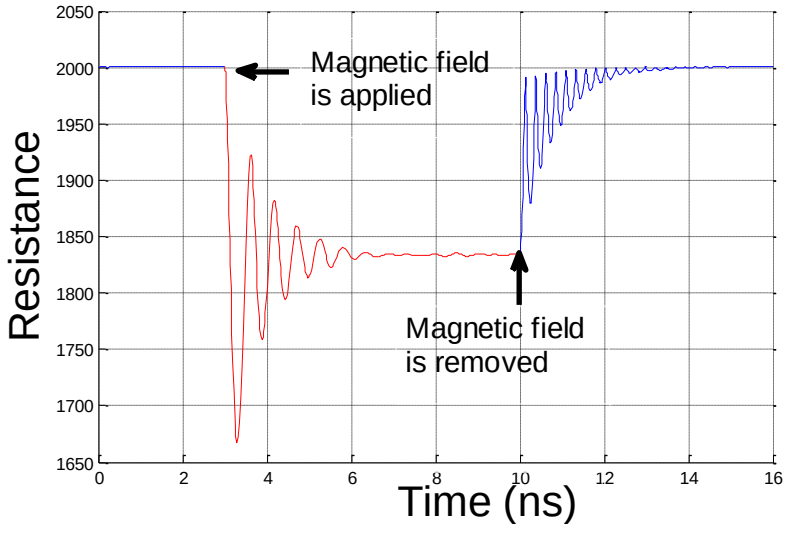

Figure 4-4: 2D motion of magnetization under magnetic field

magnetization, it reaches a stable point after the oscillation. Applying a read current, magnitude of the external magnetic field and thermal fluctuations increase the large oscillation momentum actually which means that the possibility of flipping the resistance state of the MTJ will also be increased. Figure 4.5 shows that even though same amount of read current and external magnetic field with the Figure 4.4 is applied, since high ambient temperature also causes oscillation, MTJ flips to low resistance.

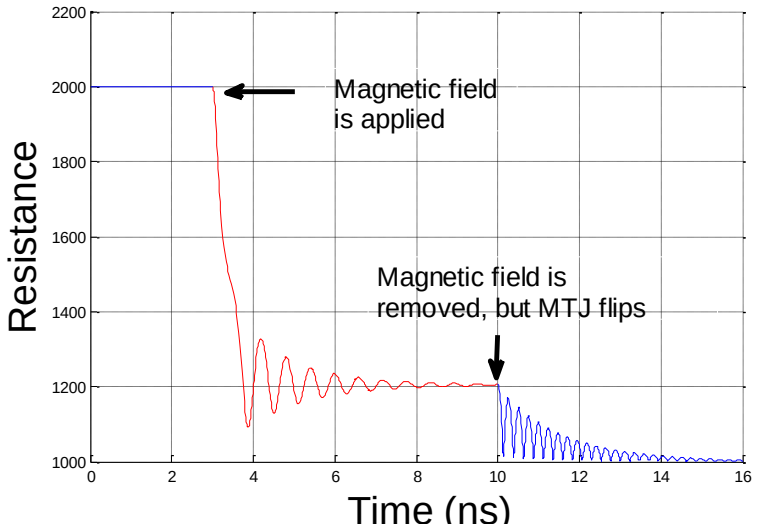

Figure 4-5: Inadvertently flipping of MTJ due to thermal noise.

4.1.3 Sensing Margin of FA-STT

Figure 4.6 shows the relationship between amplitude of external magnetic field vs. oscillation range and sensing margin in read '0' and '1' respectively. As shown in Figure 4.4, free layer's

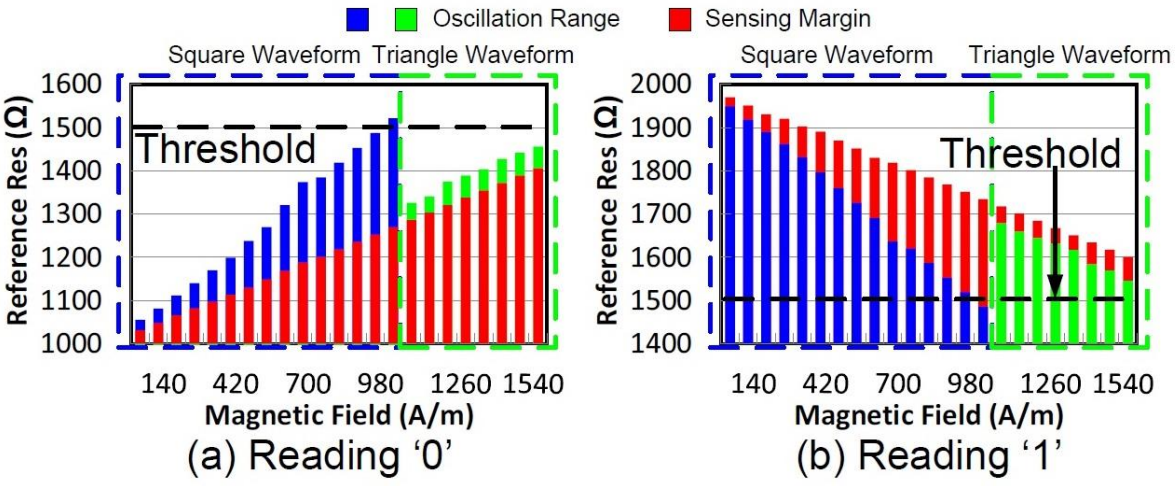

Figure 4-6: (a) Resistance changes in reading '0'. (b) Resistance changes in reading '1'.

magnetization reaches the sensing margin after some oscillation. Magnitude of the magnetic field is sweeps within the range that the MTJ state will not be flipped even considering the worst-case thermal fluctuations.

Here we considered two scenarios: first scenario, control transistor R_{en2} is turned on sharply by a step signal, second scenario, slowly turn on the transistor R_{en2} with a gradually increased control signal.

The difference between the stable intermediate state of the MTJ resistance and the original resistance state (i.e., 1000Ω in Figure 4.6(a) and 2000Ω in Figure 4.6(b), respectively) reflects the sense margin under specific magnetic field magnitude.

In first scenario, because of the large oscillation momentum, in both cases, sense margin is limited less than 200Ω.

In order to minimize the oscillation range generated by external magnetic field and increase the sense margin, we prefer to use second scenario: slowly turn on the transistor R_{en2} as shown in Figure 4.7.

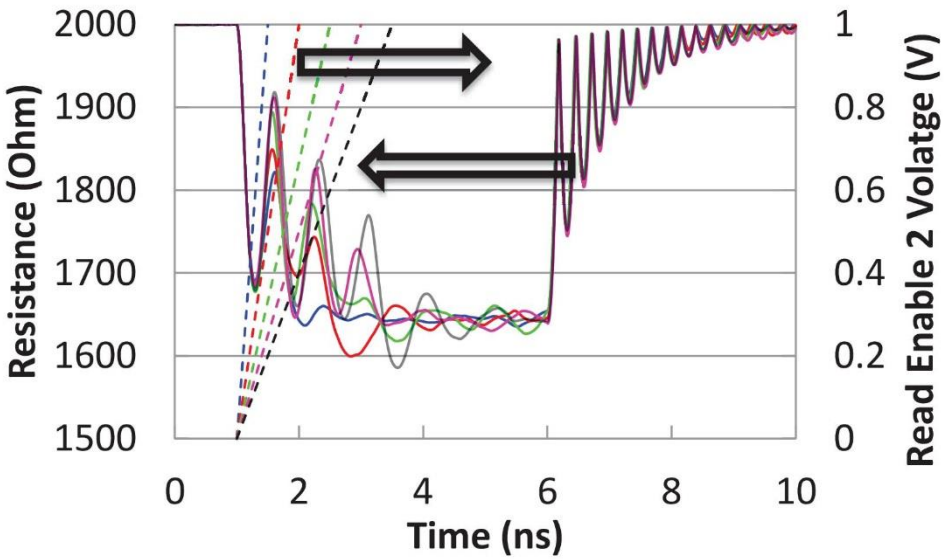

Figure 4-7: MTJ resistance change under different magnetic field applying speed.

Our simulation results show that by extending the slope of the R_{en2} control signal to 3ns, the sense margin of FA-STT sensing scheme can be safely raised to 350Ω.

To evaluate the impact of read error rates in different sensing schemes on memory array yield, Monte-Carlo simulations are conducted to obtain the sense margin distribution of three sensing schemes FA-STT sensing (FA-STT), conventional nondestructive self-reference sensing (CN) [15], and conventional STT sensing (CS), which directly compares the MTJ resistance with a reference of $(R_L + R_H)/2$. We adopted a low read current (20μA) in all three sensing schemes to ensure a negligible read disturbance rate.

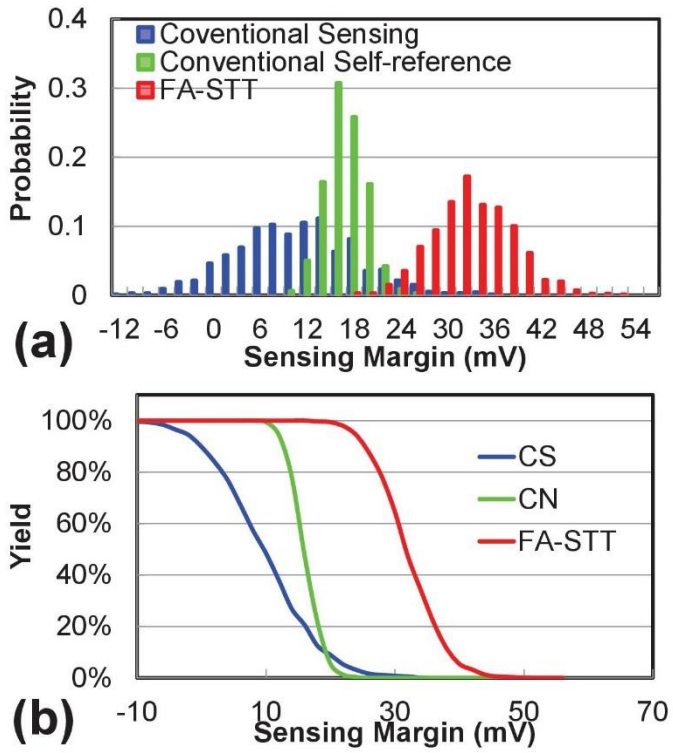

Figure 4-8: (a) Sensing margin distributions. (b) Memory yields vs. sensing margins.

Figure 4.8(a) shows the sense margin distributions of different sensing schemes. In conventional STT sensing (CS), as the R_L (R_H) of some MTJs are higher (lower) than the reference value, negative sensing margins appear in the distribution, resulting in false detection of the STT-RAM cell data. However, because of the nature of self-referencing, CN and FA-STT always produce positive sensing margin for all STT-RAM cells. Although FA-STT sensing has a wider sense margin distribution than CN sensing, it still offer better read reliability due to the significantly improved sense margin.

Figure 4.8(b) shows the memory yields of different sensing scheme under different minimum sense margin requirements. CS sensing has the lowest memory yield among all sensing schemes. Both CN and FA-STT sensing schemes demonstrates a high yield when the required sense

margin is small. The yield of CN sensing, however, drops quickly when sense margin required raises beyond 10mV. As a comparison, FA-STT can tolerate a minimum sense margin requirement of more than 20mV, which is doubled from the one of CN sensing scheme, for a memory yield of 99.99% [16].

4.2 FA-STT WRITE SCHEME

The external magnetic field introduced in FA-STT design can also accelerate the MTJ switching speed during the write operation of STT-RAM cells. Figure 4.9 shows the magnetization motion of the MTJ free layer when a standard STT-RAM cell switches from '1' to '0', a FA-STT cell switches from '1' to '0' and '0' to '1', respectively.

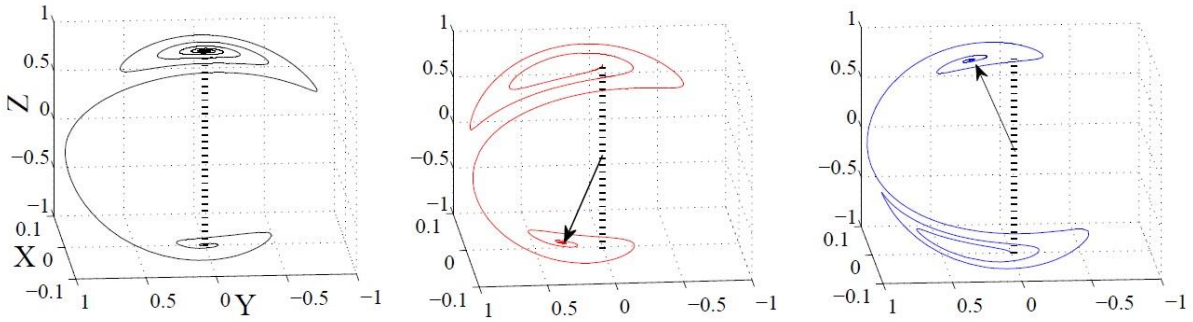

Figure 4-9: (a)Standard STT-RAM '1' to '0' (b)FA-STT '1' to '0' (c)FA-STT '0' to '1'

Here the external magnetic field is applied on the FA-STT cell during the write operations. By comparing these three figures, it can be easily observed that the external magnetic field accelerates the convergence of the magnetization oscillation and speeds up the MTJ resistance switching.

In our simulation, all ‘1’ to ‘0’ switching starts at coordinates (x, y, z) = (0, 0, 1). The ‘1’ to ‘0’ switching of the standard STT-RAM cell ends at (0, 0,-1). The ‘1’ to ‘0’ switching of the FA-STT cell, however, ends at (0, 0.3, -0.95) under the influence of the applied external magnetic field. The magnetization orientation of the MTJ free layer in the FA-STT cell goes back to (0, 0, -1) only when the external magnetic field is removed after the write operation completes. A similar scenario happens in the ‘0’ to ‘1’ switching too.

The external magnetic field accelerates the MTJ switching by turning the magnetization orientation of the free layer toward 90^{o} relevant to its initial position, no matter of it is initially parallel or anti parallel to the magnetization orientation of the reference layer. However, after magnetization orientation of the free layer crosses over 90^{o}, the external magnetic field start to hinder the stabilization of the new MTJ resistance state. Hence, applying external magnetic field throughout the entire write operation might not be necessary. Based on the MTJ switching theory, after the magnetization orientation of the free layer crosses over 90^{o}, a small amount of switching current is sufficient to retain the switching momentum and complete the switching. Thus, the external magnetic field may be removed earlier then the write current pulse to improve the write performance and save the write energy [16].

4.2.1 Write Performance Evaluation

Mean of the MTJ switching time under different magnetic field magnitudes can be seen in Figure 4.10(a). In our simulation, we observed that, as the magnetic field increases, the MTJ switching time decreases first and then becomes saturated. The variations of the switching time

is measured by the standard deviation over mean ration (SDMR), which is shown in Figure 4.10(b).

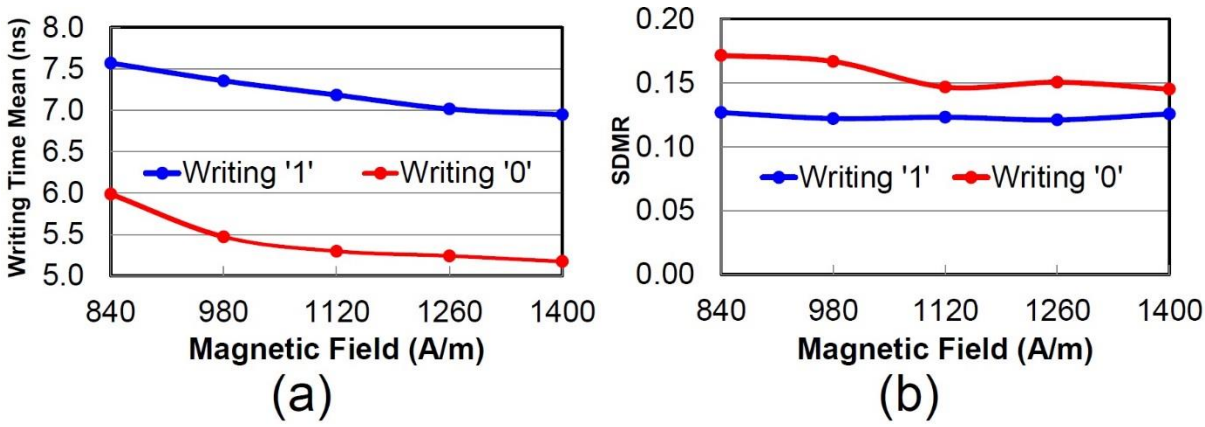

Figure 4-10: (a) The mean of MTJ switching time (b) The SDMR of MTJ switching time

In general, the variation of the MTJ switching time in writing '1' keeps constant while that in writing '0' decreases slightly as the magnetic field increases. Also writing '1' has a smaller SDMR than writing '0', mainly because writing '1' has a smaller nominal value of MTJ switching time. Considering both write performance and its variation, we choose 1.26×10^3 A/m as the optimal magnitude of the external magnetic field in the following simulations.

Figure 4.11 shows the distribution of STT-RAM write time obtained from Monte-Carlo simulations. We assume that the select transistor in the STT-RAM cell has a dimension of W/L=180nm/45nm and include both process variations and thermal randomness. Three designs were compared, including: (a) the standard STT-RAM, (b) the FA-STT with 8ns of magnetic field, and (c) the FA-STT with 4 ns of magnetic field. The write time is defined as the time period for the free layer completely switches its magnetization to the parallel or anti-parallel state. In the figures, the distributions of writing '0' and writing '1' are given separately.

Compared with the standard STT-RAM design, the magnetic field in FA-STT dramatically improves the write speed as well as reduces the variations in write time. Furthermore, the asymmetric writes in the standard STT-RAM design (i.e., writing '1' is much harder and requires longer time than writing '0') is relaxed in FA-STT. For example, as shown in Figure 4.11(b_1) and (b_2), writing '1' and '0' in FA-STT with 8ns assisting field have the similar write time and corresponding distributions. Reducing the assisting field to 4ns makes writing '1' and

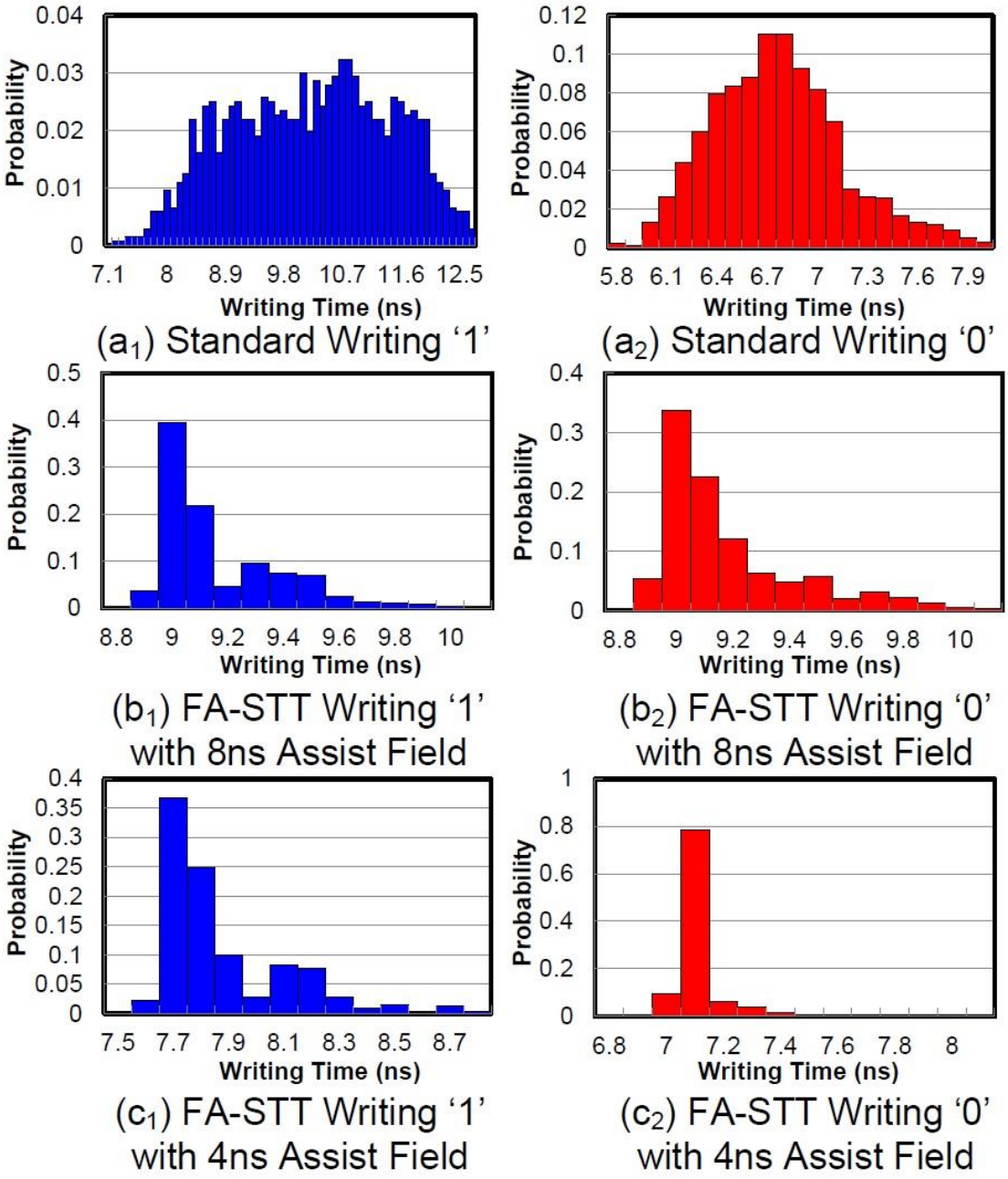

Figure 4-11: Write time distribution

'0' in FA-STT a little unbalanced, as shown in Figure 4.11(c1) and (c2). This is because the duration of the magnetic field occupies smaller portion of the total write time, resulting less

contribution to the MTJ switching. Nonetheless, the small difference between the results of 4ns and 8ns magnetic field indicates that 4 ns is sufficient for MTJ switching assistance.

4.2.2 Write Error Rate

Table 4.1 compares the write error rates of the above three STT-RAM designs, assuming a fixed 10ns write period and NMOS select transistor of W/L =180nm/45nm.

Table 4-1 Comparison of write error rates under 10ns write period.

	Writing '1'	Writing '0'
Standard STT-RAM	0.42	2.05×10^{-5}
FA-STT with 8ns Assisted Field	3.68×10^{-4}	9.60×10^{-5}
FA-STT with 4ns Assisted Field	2.29×10^{-9}	5.45×10^{-14}

In the standard STT-RAM, the errors of writing '1' dominates the write errors, i.e., a 42% error rate that is unaffordable in real design. Raising the transistor size and/or prolonging the write period become necessary to ensure a reliable write with an acceptable error rate. Compared with the standard STT-RAM, FA-STT with 8ns magnetic field reduces the error rate by three-orders-of-magnitude in writing '1'. The writing '0' error rate slightly increases because the assisted field lasts too long. Decreasing the magnetic field to 4ns dramatically reduces the error

rates in writing ‘1’ and writing ‘0’ down to 2.29 x 10^{-9} and even lower. Relaxing the write error requirement can further improve the write speed or reduce the STT-RAM cell area.

4.3 LAYOUT DESIGN CONSODERATION

In FA-STT design, a metal wire is placed above the STT-RAM cells to generate the external magnetic field. How to calculate the magnitude of the external magnetic field is explained in Part 4.5.

To minimize the required magnitude of the current, the metal wire should be placed close to the MTJ. Figure 4.12(a) and (b) show two options of the wire placement by assuming the MTJ is fabricated between metal 1 and metal 2: (1) the metal wire is placed at metal 1 between the source and the drain of the transistor; and (2) the metal wire is placed at metal 3 on top of the MTJ.

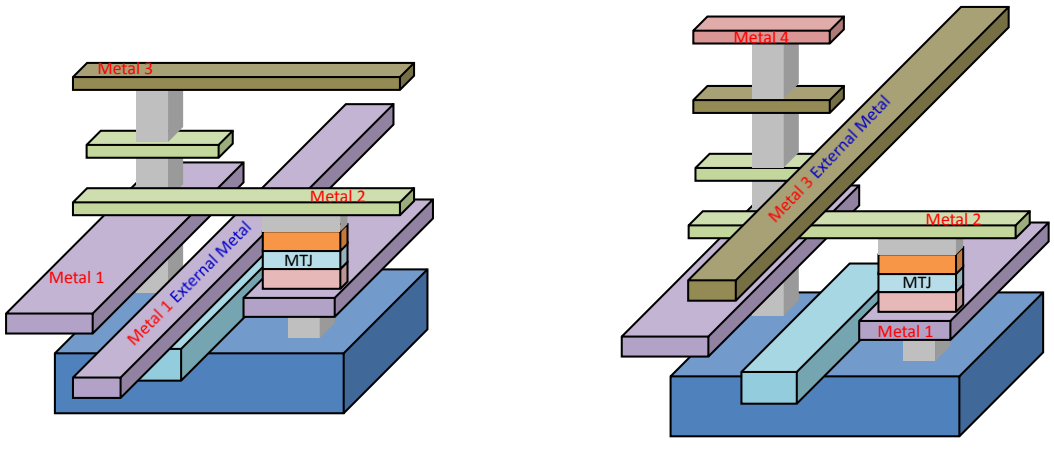

(a) (b)

Figure 4-12: 3D View of external metal placing

The magnitude of the current required to generate a magnetic field of 1.26×10^3 A/m is 782μA in Figure 4.12(a) and 2.6mA in Figure 4.12(b), respectively, assuming 10% variation tolerance.

However, according to the design rule of 45nm technology, there is not enough space to place a sufficiently wide metal wire for the required current magnitude with a W/L=180nm/45nm select transistor in option (1). Hence, option (2) is chosen in our FA-STT design and the corresponding layout is shown in Figure 4.13.

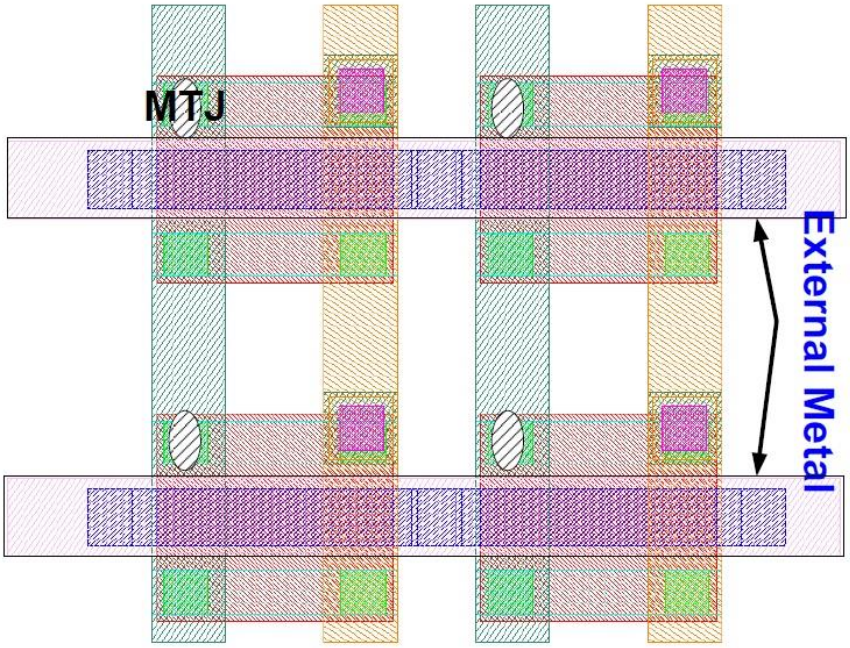

Figure 4-13: Layout design of FA-STT.

According to wire width requirements of ITRS **Error! Reference source not found.**, we are able to fit a sufficiently wide metal wire into this layout structure to carry a current of 2.6mA.

This structure, however, requires at least 4 metal layers in the STT-RAM array area by reserving one metal layer solely for the wires generating the magnetic field. Note that although option (2) is selected in our FA-STT design, option (1) may be still utilized for read/write energy reduction if a wide transistor size is adopted in STT-RAM cell designs, e.g., a multi-level cell structure.

4.4 MTJ VARIATIONS

MTJ variations can be classified into two groups MTJ size and thermal fluctuations. Langevin random field is representing thermal noise in the MTJ switching [11]

$$h_{L,\mathrm{i}} = \sqrt{\frac{2\alpha k_B T}{\gamma M_s V}} X_i(\mathrm{t}), (\mathrm{i} = \mathrm{x}, \mathrm{y}, \mathrm{z}) \tag{4.8}$$

Here T is the temperature, V is the geometry volume of free layer. $X_i(t)$ is a Gaussian random noise on x,y,z axis. As can be seen from the equation, MTJ size mainly affect the Langevin random filed h_L. h_L is inversely proportional to the square root of the MTJ free layer volume V which equals the product of the MTJ surface area A and the free layer thickness lm. Hence it can be represented as;

$$h_L \propto \frac{1}{\sqrt{A \times l_m}} \tag{4.9}$$

It indicates that a large MTJ surface area and or a thick free layer can help to minimize the variation of MTJ switching performance incurred by thermal fluctuations.

Effective spin torque term is also affected by MTJ size as shown in equation

$$h_s = \frac{(\frac{\hbar}{2e})\eta \mathrm{I}}{l_m a^2 M_s H_k} \tag{4.10}$$

h_S is inverse proportional area A and thickness lm

$$h_s \propto \frac{1}{A \times l_m} \tag{4.11}$$

It means that the efficiency of the spin current for MTJ switching is higher in a small size MTJ than in a large one. For the size variation we assumed area A variation is about 5% and thickness is 5%. Based on this MTJ size variation, effective spin torque term can be calculated as;

$$h_s = \frac{(\frac{\hbar}{2e})\eta \mathrm{I}}{H_k M_s((a^2 - \alpha^2 * \mathrm{MTJvariation}) * (\mathrm{l}_m - \mathrm{l}_m * \mathrm{MTJvariation}))} \tag{5.12}$$

4.5 DETERMINING VALUE OF CURRENT FOR MAGNETIC FIELD

Amplitude of the external magnetic field created by injecting a current to the metal layer which will be used for read and write operation can be calculated by Biot-Savart law. Based on the Biot-Savart law, magnetic field can be calculated by this equation 4.13.

$$dH = \frac{1}{4\pi} \frac{I d\vec{l} \times \vec{r}_0}{r^2}. \tag{4.13}$$

in which $\vec{r}_0$ is the unit vector between metal layer and MTJ, $d\vec{l}$ is the vector for the differential element of the metal layer and r is the distance between metal layer and the MTJ. Since in

respect to MTJ, metal layer will be very long, after integrating from positive infinite to negative infinite, equation (4.13) can be written as this form;

$$H = \frac{I}{2\pi r}. \tag{4.14}$$

In which I is the current injected to metal layer and r is the distance between these two. For obtaining maximum magnetic field, metal layer should be placed top of the MTJ as diagonal. In the layout, MTJ will be placed between metal layer1 and 2. So metal layer 3 can be used to create magnetic field. In this situation the distance between metal layer 3 and MTJ will be 300 nm [12]. Since the required magnetic field is between 0.7×10^{3} A/m and 1.33×10^{3} A/m, corresponding current will be 1.3mA and 2.5mA, respectively.

5.0 METHODOLOGY

In our work, we used MATLAB based MTJ model to conduct the relevant simulations and analyze the effect of different parameters such as thermal fluctuation, device size variation and high and low resistance variation of the MTJ for the FA-STT. In addition, we observed how free layer's magnetic moment reacts under the influence of an external magnetic field. Free layer's magnetic moment's 3D motion can be explicitly simulated using our model. Furthermore, we used our model for collecting the MTJ resistance value used to calculate the sense margin of STT-RAM read operation and obtain the switching time by considering different parametric variations.

In section 5.1, we gave detailed information how to derive MTJ model by using Landau – Lifshitz - Gilbert (LLG) equation. The values of the parameters used in our work are also presented. In section 5.2, we summarize the parameters used in circuit-level simulation and how to perform circuit based simulations. The MATLAB code of our model can be found in Appendix.

5.1 MATHEMATICAL DEVELOPMENT OF THE LLG EQUATION

The time domain response of a small magnetic moment because of the applied magnetic field is modeled by the Landau – Lifshitz - Gilbert (LLG) equation. In this section we will solve the LLG equation. Hence a free layer's magnetic moment's magnitude is constant and does not change in time, using a spherical coordinate system instead of using Cartesian coordinate system makes easier the solution. The magnetic moment in the spherical coordinate system can be seen in Figure 5.1.

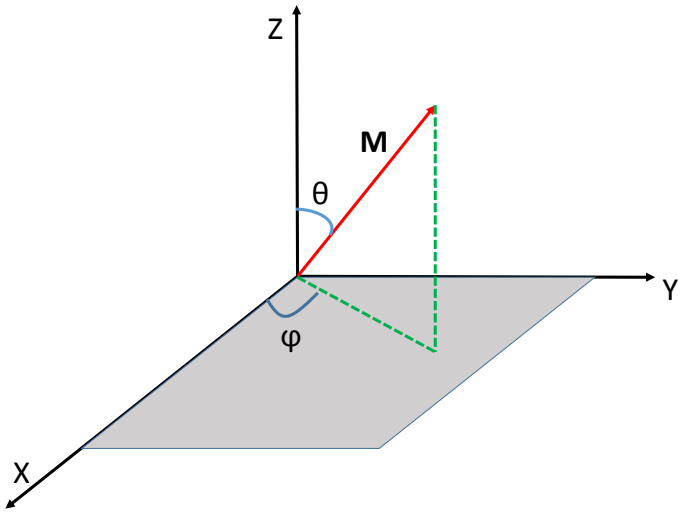

Figure 5-1: Magnetization vector in the spherical coordinate system

M can be defined as;

$$\mathbf{M} = \begin{bmatrix} M_s \sin\theta\cos\varphi\hat{\mathbf{x}} \\ M_s \sin\theta\sin\varphi\hat{\mathbf{y}} \\ M_s \cos\theta\hat{\mathbf{z}} \end{bmatrix}. \tag{5.1}$$

In which, M_s is the magnitude of the **M** and **M** changes with time as [7]

$$\frac{d\mathbf{M}}{dt} = \frac{\partial \mathbf{M}}{\partial \mathrm{M}_S}\frac{d\mathrm{M}_S}{dt} + \frac{\partial \mathbf{M}}{\partial \theta}\frac{d\theta}{dt} + \frac{\partial \mathbf{M}}{\partial \varphi}\frac{d\varphi}{dt} \tag{5.2}$$

Unit vectors of the spherical coordinate system include the partial derivatives as;

$$\hat{e}_m = \frac{\dfrac{\partial \mathbf{M}}{\partial \mathrm{M}_S}}{\left|\dfrac{\partial \mathbf{M}}{\partial \mathrm{M}_S}\right|} \tag{5.3}$$

$$\left|\frac{\partial \mathbf{M}}{\partial \mathrm{M}_S}\right| = \sqrt{\sin^2\theta\cos^2\varphi + \sin^2\theta\sin^2\varphi + \cos^2\theta} = 1 \tag{5.4}$$

$$\hat{e}_m = \frac{\partial \mathbf{M}}{\partial \mathrm{M}_S} \tag{5.5}$$

In the same manner, unit vector in respect to the θ can be derived as;

$$\hat{e}_\theta = \frac{\dfrac{\partial \mathbf{M}}{\partial \theta}}{\left|\dfrac{\partial \mathbf{M}}{\partial \theta}\right|} \tag{5.6}$$

$$\left|\frac{\partial \mathbf{M}}{\partial \theta}\right| = \sqrt{\mathrm{M}_S{}^2\cos^2\theta\cos^2\varphi + \mathrm{M}_S{}^2\cos^2\theta\sin^2\varphi + \mathrm{M}_S{}^2\sin^2\theta} = \mathrm{M}_S \tag{5.7}$$

$$\mathrm{M}_S\hat{e}_\theta = \frac{\partial \mathbf{M}}{\partial \theta} \tag{5.8}$$

and finally, unit vector in respect to the φ can be derived as;

$$\hat{e}_\varphi = \frac{\dfrac{\partial \mathbf{M}}{\partial \varphi}}{\left|\dfrac{\partial \mathbf{M}}{\partial \varphi}\right|} \tag{5.9}$$

$$\left|\frac{\partial \mathbf{M}}{\partial \varphi}\right| = \sqrt{M_S{}^2 \sin^2\theta \sin^2\varphi + M_S{}^2 \sin^2\theta \cos^2\varphi} = M_S \sin\theta \tag{5.10}$$

$$M_S \sin\theta \hat{e}_\varphi = \frac{\partial \mathbf{M}}{\partial \varphi} \tag{5.11}$$

After substituting these unit vectors in the equation 5.2, one can reach that;

$$\frac{d\mathbf{M}}{dt} = \frac{dM_S}{dt}\hat{e}_m + M_S \frac{d\theta}{dt}\hat{e}_\theta + M_S \sin\theta \frac{d\varphi}{dt}\hat{e}_\varphi. \tag{5.12}$$

Gilbert form of the Landau-Lifshitz-Gilbert equation can also be written as [16];

$$\frac{d\mathbf{M}}{dt} = -\gamma_0(\mathbf{M} \times \mathbf{H}_{\text{eff}}) + \frac{\alpha}{M_S}(\mathbf{M} \times \frac{d\mathbf{M}}{dt}) \tag{5.13}$$

in which, γ_0 is the gyromagnetic constant and α is the Gilbert damping parameter and $\mathbf{H}_{\text{eff}}$ is the summation of uniaxial anisotropy, easy plane anisotropy and applied field [7], and cross production of $\mathbf{H}_{\text{eff}}$ with $\mathbf{M}$ can be written as;

$$\mathbf{M} \times \mathbf{H}_{\text{eff}} = \begin{bmatrix} \hat{e}_m & \hat{e}_\theta & \hat{e}_\varphi \\ M_S & 0 & 0 \\ \mathbf{H}_{\text{eff}}\hat{e}_m & \mathbf{H}_{\text{eff}}\hat{e}_\theta & \mathbf{H}_{\text{eff}}\hat{e}_\varphi \end{bmatrix} \tag{5.14}$$

$$= -M_S(\mathbf{H}_{\text{eff}}\hat{e}_\varphi)\hat{e}_\theta + M_S(\mathbf{H}_{\text{eff}}\hat{e}_\theta)\hat{e}_\varphi \tag{5.15}$$

And

$$\mathbf{M} \times \frac{d\mathbf{M}}{dt} = \begin{bmatrix} \hat{e}_m & \hat{e}_\theta & \hat{e}_\varphi \\ M_S & 0 & 0 \\ \frac{dM_S}{dt} & M_S\frac{d\theta}{dt} & M_S \sin\theta \frac{d\varphi}{dt} \end{bmatrix} \tag{5.16}$$

$$= -M_S{}^2 \sin\theta \frac{d\varphi}{dt}\hat{e}_\theta + M_S{}^2 \frac{d\theta}{dt}\hat{e}_\varphi \tag{5.17}$$

Substituting the equation 5.15 and 5.17 in equation 5.13, one can reach that

$$\frac{d\mathbf{M}}{dt} = -\gamma_0(-\mathrm{M}_S(\mathbf{H}_{\mathrm{eff}}\hat{e}_\varphi)\hat{e}_\theta + \mathrm{M}_S(\mathbf{H}_{\mathrm{eff}}\hat{e}_\theta)\hat{e}_\varphi) + \frac{\alpha}{\mathrm{M}_S}(-\mathrm{M}_S{}^2\sin\theta\frac{d\varphi}{dt}\hat{e}_\theta + \mathrm{M}_S{}^2\frac{d\theta}{dt}\hat{e}_\varphi) \quad (5.18)$$

After putting equation 5.12 and 5.18 in matrix form, we can reach that,

$$\begin{bmatrix} \frac{d\mathrm{M}_S}{dt}\hat{e}_m \\ \mathrm{M}_S\frac{d\theta}{dt}\hat{e}_\theta \\ \mathrm{M}_S\sin\theta\frac{d\varphi}{dt}\hat{e}_\varphi \end{bmatrix} = \begin{bmatrix} 0 \\ (\gamma_0\mathrm{M}_S(\mathbf{H}_{\mathrm{eff}}\hat{e}_\varphi) - \alpha\mathrm{M}_S\sin\theta\frac{d\varphi}{dt})\hat{e}_\theta \\ (-\gamma_0\mathrm{M}_S(\mathbf{H}_{\mathrm{eff}}\hat{e}_\theta) + \alpha\mathrm{M}_S\frac{d\theta}{dt})\hat{e}_\varphi \end{bmatrix} \quad (5.19)$$

In this equation, $\mathbf{H}_{\mathrm{eff}}$ must be opened. $\mathbf{H}_{\mathrm{eff}}$ can be defined as [18];

$$\mathbf{H}_{\mathrm{eff}} = -\frac{1}{\mu_0\mathrm{V}}\frac{\partial\mathrm{E}}{\partial\mathbf{M}} \quad (5.20)$$

in which E is the energy (such as uniaxial anisotropy, easy plane anisotropy, magnetic field). After substituting this term in $\gamma_0\mathrm{M}_S(\mathbf{H}_{\mathrm{eff}}\hat{e}_\varphi)$ and in $-\gamma_0\mathrm{M}_S(\mathbf{H}_{\mathrm{eff}}\hat{e}_\theta)$, equation 5.19 will be

$$\begin{bmatrix} \frac{d\mathrm{M}_S}{dt}\hat{e}_m \\ \mathrm{M}_S\frac{d\theta}{dt}\hat{e}_\theta \\ \mathrm{M}_S\sin\theta\frac{d\varphi}{dt}\hat{e}_\varphi \end{bmatrix} = \begin{bmatrix} 0 \\ (-\frac{\gamma_0}{\mu_0\mathrm{V}\sin\theta}\frac{\partial\mathrm{E}}{\partial\varphi} - \alpha\mathrm{M}_S\sin\theta\frac{d\varphi}{dt})\hat{e}_\theta \\ (\frac{\gamma_0}{\mu_0\mathrm{V}}\frac{\partial\mathrm{E}}{\partial\theta} + \alpha\mathrm{M}_S\frac{d\theta}{dt})\hat{e}_\varphi \end{bmatrix} \quad (5.21)$$

After this step, we can reach two one order differential equations as follows;

$$\mathrm{M}_S\frac{d\theta}{dt} = -\frac{\gamma_0}{\mu_0\mathrm{V}\sin\theta}\frac{\partial\mathrm{E}}{\partial\varphi} - \alpha\mathrm{M}_S\sin\theta\frac{d\varphi}{dt} \quad (5.22)$$

$$\mathrm{M}_S\sin\theta\frac{d\varphi}{dt} = \frac{\gamma_0}{\mu_0\mathrm{V}}\frac{\partial\mathrm{E}}{\partial\theta} + \alpha\mathrm{M}_S\frac{d\theta}{dt} \quad (5.23)$$

Substituting equation 5.23 in equation 5.22, we can get the equation 5.24 as follow

$$\frac{d\theta}{dt} = \frac{\gamma_0}{\mu_0 V M_S (1+\alpha^2)}\left[-\frac{1}{\sin\theta}\frac{\partial E}{\partial \varphi} - \alpha\frac{\partial E}{\partial \theta}\right] \tag{5.24}$$

Substituting equation 5.22 in equation 5.23, we can get the equation 5.25 as follow

$$\frac{d\varphi}{dt} = \frac{\gamma_0}{\mu_0 V M_S (1+\alpha^2)}\frac{1}{\sin\theta}\left[-\frac{\alpha}{\sin\theta}\frac{\partial E}{\partial \varphi} + \frac{\partial E}{\partial \theta}\right] \tag{5.25}$$

The effective fields can also be defined by θ and φ as follows [7][19];

$$H_\theta = -\frac{1}{\mu_0 V M_S}\frac{\partial E}{\partial \theta} \text{ and } H_\varphi = -\frac{1}{\mu_0 V M_S \sin\theta}\frac{\partial E}{\partial \varphi}. \tag{5.26}$$

After substituting these fields in equation 5.24 and 5.25, we can reach the final form of the equation as follows:

$$\frac{d\theta}{dt} = \frac{\gamma_0}{(1+\alpha^2)}\left[H_\varphi + \alpha H_\theta\right] \tag{5.27}$$

$$\frac{d\varphi}{dt} = \frac{\gamma_0}{(1+\alpha^2)}\frac{1}{\sin\theta}\left[\alpha H_\varphi - H_\theta\right] \tag{5.28}$$

The rest of the work will be about finding H_θ and H_φ for different energies such as uniaxial anisotropy, easy plane anisotropy, Zeeman energy (incurred applied magnetic field). We can start the calculation by uniaxial anisotropy. Uniaxial anisotropy is defined as [14];

$$E_K = KV\sin^2\theta \tag{5.29}$$

in which K is material dependent uniaxial anisotropy constant. After using the definition of effective fields (equation 5.26), one can reach that;

$$H_{K\theta} = -\frac{2K\sin\theta\cos\theta}{\mu_0 M_S} \text{ and } H_{K\varphi} = 0. \tag{5.30}$$

Easy plane anisotropy is defined as [11];

$$E_P = K_P V(\sin^2\theta\cos^2\varphi - 1) \tag{5.31}$$

and effective fields for easy plane can be calculated as;

$$H_{P\theta} = -\frac{2K_P \sin\theta\cos\theta\cos^2\varphi}{\mu_0 M_S} \text{ and } H_{P\varphi} = \frac{2K_P \sin\theta\cos\varphi\sin\varphi}{\mu_0 M_S} \quad . \tag{5.32}$$

Applied magnetic field energy is also known as Zeeman energy and defined as [14];

$$E_H = -\mathbf{M.H} = -MH(\sin\theta\sin\varphi\sin\psi + \cos\theta\cos\psi) \tag{5.32}$$

Effective fields for applied magnetic field can be calculated as;

$$H_{H\theta} = \frac{h(\sin\theta\cos\psi - \cos\theta\sin\varphi\sin\psi)}{\mu_0 M_S} \text{ and } H_{H\varphi} = \frac{h\cos\theta\sin\psi}{\mu_0 M_S} \tag{5.34}$$

in which, ψ is the angle of magnetic field vector and easy axis and h is normalized value of the magnitude of the magnetic field.

Langevin random field related to the temperature can be expressed as [11];

$$H_{L\theta} = h_{l,z}\sin\theta - \cos\theta(h_{l,x}\cos\varphi + h_{l,y}\sin\varphi) \text{ and } H_{L\varphi} = h_{l,y}\cos\varphi - h_{l,x}\sin\varphi \tag{5.35}$$

in which, $h_{l,i} = \sqrt{\frac{2\alpha k_B T}{\gamma M_S V}} X_i(t).(i = x, y, z)$. α Gilbert damping constant, k_B Boltzmann constant, T temperature, γ gyromagnetic constant, and V is the volume of the free layer. The effective spin torque term can be written as [11];

$$H_{S\theta} = h_S \sin\theta \text{ and } H_{S\varphi} = h_S \tag{5.36}$$

in which h_S is normalized effective spin torque. Now we can combine all of the effective fields in equation 5.37 and 5.38 as follows;

$$\frac{d\theta}{dt} = \frac{\gamma_0}{(1+\alpha^2)}\left[H_{K\varphi} + H_{P\varphi} + H_{H\varphi} + H_{L\varphi} + H_{S\varphi} + \alpha(H_{K\theta} + H_{P\theta} + H_{H\theta} + H_{L\theta} + H_{S\theta})\right] \tag{5.37}$$

$$\frac{d\varphi}{dt} = \frac{\gamma_0}{(1+\alpha^2)}\frac{1}{\sin\theta}\left[\alpha(H_{K\varphi} + H_{P\varphi} + H_{H\varphi} + H_{L\varphi} + H_{S\varphi}) - (H_{K\theta} + H_{P\theta} + H_{H\theta} + H_{L\theta} + H_{S\theta})\right] \tag{5.38}$$

In our model we used the normalized value of the each term. Normalization quantities can be seen in Table 5.1 and the parameters which we used in our model simulation can be found in Table 5.2.

Table 5-1 Normalization table [14]

Dimensionless variable	Conversion relation	Normalization quantity
Magnetization	$\mathbf{m} = \frac{\mathbf{M}}{M_S}$	Saturation magnetization
Magnetic field	$h = \frac{H}{K}$	Uniaxial anisotropy
Easy plane anisotropy	$h_p = \frac{K_p}{K}$	Uniaxial anisotropy

Table 5-2 Model parameters table

Parameter	Symbol	Value
Permeability of free space	μ_0	$4\pi \times 10^{-7} [\frac{wb}{Am}]$
Gyromagnetic ratio of material	Γ	$1.76 \times 10^{11} [\frac{rad}{sT}]$
Gyromagnetic ratio	γ_0	$\gamma_0 = \mu_0 . \gamma, 2.21 \times 10^5 [\frac{m}{As}]$
Electron charge	E	1.602×10^{-19} c
Planck's constant	$\hbar$	1.005×10^{-34} J.s
Uniaxial anisotropy [7]	K_u	$300 [\frac{J}{m^3}]$
Easy plane anisotropy [11]	K_p	$180 [\frac{J}{m^3}]$
Spin polarization factor [7]	P	0.35
Magnetization saturation [7]	M_S	$8 \times 10^5 [\frac{A}{m}]$

Table 5-2 (continued)

Applied magnetic field	H	$1.26 \times 10^3 [\frac{A}{m}]$
Gilbert damping parameter	A	0.01
Easy axis direction		z axis, (0,0,1)

5.2 CIRCUIT SIMULATION

In our work, after developing the magnetic model and collecting data, we need to conduct the circuit based simulations. Circuit design parameters used in our simulations of the dynamic MTJ resistance change during FA-STT self-reference sensing process are summarized in Table 5.3. In our simulations, the nominal values of the parameters are adopted from [20]. Specifically, R_H and R_L are set to 2000Ω and 1000Ω, respectively. In order to avoid read, a relatively small read current (20μA) is selected.

Table 5-3 Design Parameters

Parameter	Mean	1 σ deviation
RA ($\Omega\mu m^2$)	8.1	7%
Surface Area (nm^2)	45 x 90	5% x technology node
Oxide Thickness (nm)	2.2	2%
TMR ratio	1	5%
High Resistance (R_H) (Ω)	2000	design dependent
Low Resistance (R_L) (Ω)	1000	design dependent
Reading Current (μA)	20	design dependent
Transistor Size (nm^2)	45 x 180	5% x technology node

While we are simulating the sense margin distribution (see Section 4.1.3) and write time distribution (see Section 4.2.1), we conducted 1000 times Monte-Carlo simulations based on the design parameters presented in Table 5.3. Some error rate values are estimated by the curve fitting method from [21].

6.0 CONCLUSION

In this work, we proposed FA-STT – a novel sensing scheme to overcome the large cell-to-cell variations in STT-RAM designs. By using an external magnetic field to generate the self-referenced resistive sense signal, FA-STT offers a much better read reliability (i.e., 200% higher sense margin) compared to conventional self-reference sensing schemes. The introduced magnetic field can be also utilized to assist the write operations of the STT-RAM without incurring any extra hardware cost, achieving a write error rate of 2.29×10^{-9}. The improved switching performance of the MTJ device also relaxes the requirement of select transistor driving ability, leading to a smaller STT-RAM cell area due to the reduced transistor size.

APPENDIX

MATLAB CODE OF THE MODEL

fun.m

```
function dy=fun(y,hs,hd)
a=0.01;
hp=180;
hl=0.016;
Xx=randn(1,1);
Xy=randn(1,1);
Xz=randn(1,1);
angle = pi*(1/2);

dy(1)=  (-a*sin(y(1))*cos(y(1)))+...
          (-hp*(sin(y(2))+a*cos(y(1))*cos(y(2)))*sin(y(1))*cos(y(2)))+ ...
           (hs*(-sin(y(1))))+...
           (hl*(a*((Xz*sin(y(1)))-Xx*cos(y(1))*cos(y(2))-Xy*cos(y(1))*sin(y(2)))+….
         Xy*cos(y(2))Xx*sin(y(2))))+...
         (-hd*(cos(y(2))*sin(angle) + a*(sin(y(1))*cos(angle)- cos(y(1))*sin(y(2))*sin(angle))));
         %magnetic field
 dy(2)=  (-cos(y(1)))+...
           (-hp*((cos(y(1))*cos(y(2)))-a*sin(y(2)))*cos(y(2)))+...
           (hs*a)+...
           (hl*(a*(Xx*sin(y(2))-Xy*cos(y(2)))+Xz*sin(y(2))-Xx*cos(y(1))*cos(y(2))-…
         Xy*cos(y(1))*sin(y(2)))/sin(y(1)))+...
           (-hd*(sin(y(1))*cos(angle) - cos(y(1))*sin(y(2))*sin(angle) -…
           a*cos(y(2))*sin(angle))/sin(y(1)));
dy=dy';
```

magcode.m

```
clc;
```

```
clear all;
pi=3.14;

app_field_0=8;
remove_field_0 = 15;
switch_time=24;
app_field_1=32;
remove_field_1 =38;
while(i<1)
    hold all;
    grid;
    options=odeset('RelTol',1e-04);
    MTJvariation=rand;
    hs=-0.00278*(200);
    hd=0.0;
    [t0,y]=ode113(@(t,y) fun(y,hs,hd),[0,app_field_0],[0.01,pi/2],options);
    y00=y(:,1);
    y01=y(:,2);
    if(y00<=pi+0.1)
    plot(t0,y00,'r')
    end
    T= t0==app_field_0;
    f00=removerows(y00,find(~T));
    f01=removerows(y01,find(~T));
    hs=0;
    hd=0.0;
    [t1,y]=ode113(@(t,y) fun(y,hs,hd),[app_field_0,remove_field_0],[f00,f01],options);
    y1=y(:,1);
    y2=y(:,2);
    Mz1=cos(y1);
    if(y1<= pi+0.1)
       plot(t1,y1,'green');
    end
    T= t1==remove_field_0;
    f1=removerows(y1,find(~T));
    f2=removerows(y2,find(~T));
    hs=-0.00278*(800);
    hd = 0.0;
    [t2,y]=ode113(@(t,y) fun(y,hs,hd),[remove_field_0,switch_time],[f1,f2],options);
    y3=y(:,1);
    y4=y(:,2);
    Mz3=cos(y3);
    T= t2==switch_time;
    f3=removerows(y3,find(~T));
    f4=removerows(y4,find(~T));
```

```
        if(y3<=pi+0.1)
        plot(t2,y3,'black');
        end
        hs=0;
        hd=0.0;
        [t3,y]=ode113(@(t,y) fun(y,hs,hd),[switch_time,app_field_1],[f3,f4],options);
        y5=y(:,1);
        y6=y(:,2);
        Mz5=cos(y5);
        T= t3==app_field_1;
        f5=removerows(y5,find(~T));
        f6=removerows(y6,find(~T));
        if(y5<=pi+0.1)
        plot(t3,y5,'red');
        end
        hs=0.0;
        hd=0.0;
        [t4,y]=ode113(@(t,y) fun(y,hs,hd),[app_field_1,remove_field_1],[f5,f6],options);
        y7=y(:,1);
        y8=y(:,2);
        Mz6=cos(y8);
        T= t4==remove_field_1;
        f7=removerows(y7,find(~T));
        f8=removerows(y8,find(~T));
        if(y7<=pi+0.1)
        plot(t4,y7,'green');
        end
        i=i+1;
end
```

BIBLIOGRAPHY

[1] Motoyoshi, M., I. Yamamura, W. Ohtsuka, M. Shouji, H. Yamagishi, M. Nakamura, H. Yamada et al. "A study for 0.18 μm high-density MRAM." InVLSI Technology, 2004. Digest of Technical Papers. 2004 Symposium on, pp. 22-23. IEEE, 2004.Flatte, Michael E. "Spintronics." Electron Devices, IEEE Transactions on 54, no. 5 (2007): 907-920.

[2] Kim, Jisu, Kyungho Ryu, Seung H. Kang, and Seong-Ook Jung. "A novel sensing circuit for deep submicron spin transfer torque MRAM (STT-MRAM)."Very Large Scale Integration (VLSI) Systems, IEEE Transactions on 20, no. 1 (2012): 181-186.Diao, Zhitao, Alex Panchula, Yunfei Ding, Mahendra Pakala, Shengyuan Wang, Zhanjie Li, Dmytro Apalkov et al. "Spin transfer switching in dual MgO magnetic tunnel junctions." Applied Physics Letters 90, no. 13 (2007): 132508-132508.

[3] Miltat, J., G. Albuquerque, A. Thiaville, and C. Vouille. "Spin transfer into an inhomogeneous magnetization distribution." Journal of Applied Physics 89, no. 11 (2001): 6982-6984.

[4] Liu, Yaowen, Zongzhi Zhang, Jianguo Wang, P. P. Freitas, and J. L. Martins. "Current-induced switching in low resistance magnetic tunnel junctions."Journal of applied physics 93, no. 10 (2003): 8385-8387.

[5] Xiao, Jiang, A. Zangwill, and M. D. Stiles. "Macrospin models of spin transfer dynamics." Physical Review B 72, no. 1 (2005): 014446.

[6] Lee, Jia-Mou "Nanosecond Pulse Switching in Spin-Transfer Torque Random Access Memory"

[7] Engelbrecht, Linda M. "Modeling spintronics devices in Verilog-A for use with industry-standard simulation tools." (2011).Huai, Yiming. "Spin-transfer torque MRAM (STT-MRAM): Challenges and prospects." AAPPS Bulletin 18, no. 6 (2008): 33-40.

[8] Tehrani, S., B. Engel, J. M. Slaughter, E. Chen, M. DeHerrera, M. Durlam, P. Naji, R. Whig, J. Janesky, and J. Calder. "Recent developments in magnetic tunnel junction MRAM." Magnetics, IEEE Transactions on 36, no. 5 (2000): 2752-2757.

[9] Chen, Yiran, Hai Li, Xiaobin Wang, Wenzhong Zhu, Wei Xu, and Tong Zhang. "A 130 nm 1.2 v/3.3 v 16 kb spin-transfer torque random access memory with nondestructive self-reference sensing scheme." Solid-State Circuits, IEEE Journal of 47, no. 2 (2012): 560-573.

[10] Jeong, Gitae, Wooyoung Cho, Sujin Ahn, Hongsik Jeong, Gwanhyeob Koh, Youngnam Hwang, and Kinam Kim. "A 0.24-μm 2.0-V 1T1MTJ 16-kb nonvolatile magnetoresistance RAM with self-reference sensing scheme." Solid-State Circuits, IEEE Journal of 38, no. 11 (2003):1906-1910

[11] Wang, Peiyuan, Wei Zhang, Rajiv Joshi, Rouwaida Kanj, and Yiran Chen. "A thermal and process variation aware MTJ switching model and its applications in soft error analysis." In Computer-Aided Design (ICCAD), 2012 IEEE/ACM International Conference on, pp. 720-727. IEEE, 2012.

[12] S. Natarajan, M. Armstrong, M. Bost, R. Brain, M. Brazier, C.-H. Chang et al. "A 32nm logic technology featuring 2_{nd} generation high-k + metal-gate transistors, enhanced channel strain and $0.171\mu m^2$ SRAM cell size in 291Mb Array" IEDM. Tech. Dig., Dec. 2008

[13] S. Urazhdin, R. Loloee, and W. P. Pratt, Jr. Non-collinear spin transport in magnetic multilayer. Phys.Rev.B, 71(10): 100401, Marc. 2005.

[14] Sun, J. Z. "Spin-current interaction with a mono-domain magnetic body a model study." Physical Review B62, no. 1 (2000):570

[15] Chen, Yiran, Xiaobin Wang, Wenzhong Zhu, Wei Xu, and Tong Zhang. "A nondestructive self-reference scheme for spin-transfer torque random access memory (STT-RAM)." In Design, Automation & Test in Europe Conference & Exhibition (DATE), 2010, pp. 148-153. IEEE, 2010

[16] E. Eken, Y. Zhang, W. Wen, R. Joshi, H. Li, and Y. Chen, "A New Field-assisted Access Scheme of STT-RAM with Self-reference Capability," Design Automation Conference (DAC), Jun.2014, to appear.

[17] International Technology Roadmap for Semiconductors". In http://www.itrs.net/, 2013.T. L. Gilbert, Phys. Rev. 100, 1243 (1955)

[18] M. C. Hickey. Analytical solution of the equation of motion for a rigid domain wall in a magnetic material with perpendicular anisotropy. Physical Review B, 78(18):180412, November 2008.

[19] A. Nigam, C.W. Smullen, V. Mohan, E. Chen, S. Gurumurthi, and M.R. Stan, "Delivering on the promise of universal memory for spin-transfer torque RAM (STT-RAM)", ISLPED, pp. 121-126, Aug, 2011

[20] Y. Chen, H. (Helen) Li, X. Wang, W. Zhu, W. Xu, and T. Zhang. "A Nondestructive Self-reference Scheme for Spin-Transfer Torque Random Access Memory (STT-RAM)". In Design, Automation Test in Europe, pages 148-153, 2010.

[21] Kanj, Rouwaida, Rajiv Joshi, and Sani Nassif. "Mixture importance sampling and its application to the analysis of SRAM designs in the presence of rare failure events." In Proceedings of the 43rd annual Design Automation Conference, pp. 69-72. ACM, 2006.